

Structure-preserving nodal DG method for the Euler equations with gravity: well-balanced, entropy stable, and positivity preserving

Yuchang Liu¹, Wei Guo², Yan Jiang³, and Mengping Zhang⁴

Abstract: We propose an entropy stable and positivity preserving discontinuous Galerkin (DG) scheme for the Euler equations with gravity, which is also well-balanced for hydrostatic equilibrium states. To achieve these properties, we utilize the nodal DG framework and carefully design the source term discretization using entropy conservative fluxes. Furthermore, we demonstrate that the proposed methodology is compatible with a positivity preserving scaling limiter, ensuring positivity of density and pressure under an appropriate CFL condition. To the best of our knowledge, this is the first DG scheme to simultaneously achieve these three properties with theoretical justification. Numerical examples further demonstrate its robustness and efficiency.

Key Words: balance laws, discontinuous Galerkin method, well-balanced, entropy stability, positivity-preserving.

1 Introduction

In this paper, we focus on the simulation of the Euler equations with gravity, which have broad applications in astrophysics and atmospheric science. The development of high-order methods has enabled the computation of high-resolution solutions of partial differential equations (PDEs) with fewer meshes. Among them, the discontinuous Galerkin (DG) method, introduced by Reed and Hill in 1973 [30] and later refined and extended by Cockburn and Shu in a series of seminal works [10, 9, 8, 11], offers several distinctive advantages, such as local conservation, high-order accuracy, flexibility in handling complex geometries and general boundary conditions, as well as ease of adaptation and parallel implementation. While DG discretization is an excellent tool for solving the Euler equations with gravity, such a system possesses fundamental physical structures

¹School of Mathematical Sciences, University of Science and Technology of China, Hefei, Anhui 230026, P.R. China. E-mail: lissandra@mail.ustc.edu.cn.

²Department of Mathematics and Statistics, Texas Tech University, Lubbock, TX, 79409, USA. E-mail: weimath.guo@ttu.edu. Research supported by Air Force Office of Scientific Research FA9550-18-1-0257.

³School of Mathematical Sciences, University of Science and Technology of China, Hefei, Anhui 230026, P.R. China. E-mail: jiangy@ustc.edu.cn. Research supported by NSFC grant 12271499.

⁴School of Mathematical Sciences, University of Science and Technology of China, Hefei, Anhui 230026, P.R. China. E-mail: mpzhang@ustc.edu.cn.

that must be carefully preserved to ensure reliable and robust simulations. Over the past few decades, designing structure-preserving schemes, which maintain key physical properties in the discrete sense, has become a research focus and posed a significant challenge [31]. This paper aims to develop a provably structure-preserving DG scheme for the Euler equations with gravity.

Mathematically, the Euler equations with gravity form a nonlinear balance law. A balance law admits a special class of solutions known as *equilibrium solutions* or *steady-state solutions*. At the PDE level, for these solutions, the flux term is exactly balanced by the source term, ensuring that the equilibrium state remains unchanged as time progresses. In the algorithm design, the goal is to ensure that the scheme preserves this property at the discrete level, capturing the “numerical equilibrium solutions”. Such methods, known as well-balanced (WB) schemes, offer several desired advantages. For example, even on relatively coarse meshes, WB schemes can effectively capture small perturbations added to the equilibrium state, whereas non-WB methods often fail to do so, leading to significant errors or computational instability. Many successful WB schemes have been proposed in the literature, most of which are for the shallow water equations over non-flat bottom topographies – another important class of hyperbolic balance laws, see, e.g., [38, 37, 3, 29, 12]. WB schemes for the Euler equations with gravity include, e.g., [5, 19, 39, 2]. In particular, under the DG framework, the primary technique for ensuring the WB property is to carefully modify the discretization of the source term in such a way that the flux term and source term are exactly balanced in a discrete sense. In [25], Li and Xing proposed a WB DG method for isothermal hydrostatic balance. In [6], Chandrashekar and Zenk developed a nodal DG scheme that is WB for both isothermal and isentropic hydrostatic balances, utilizing an interpolation property of the numerical solution. In [35], by using the properties of the HLLC flux, Wu and Xing developed a WB DG method for arbitrary hydrostatic equilibrium. More recently, in [14], Du, Yang, and Zhu proposed a DG method that is also WB for arbitrary hydrostatic equilibrium, utilizing the Lax-Friedrichs flux with an adjusted dissipation coefficient.

Moreover, for hyperbolic conservation laws, the entropy condition is crucial for well-posedness analysis, ensuring that the total entropy does not increase over time, in accordance with the second law of thermodynamics. Hence, it is desirable for the numerical solution to satisfy a discrete form of the entropy condition. Schemes that achieve this property are referred to as entropy-stable *entropy stable* (ES) schemes. In recent years, the development of ES methods has attracted considerable research interest. Regarding the DG discretization, there exist two primary approaches for achieving entropy stability. The first approach [7, 28, 27] relies on the construction of summation-by-parts (SBP) operators and the application of the flux differencing technique. The second approach [1, 15, 26] attempts to directly control entropy production by incorporating an artificial term into the DG formulation. A simple yet important observation made in [13] is that the Euler equations with gravity and those without a source term share the same entropy pair and entropy condition, which is useful for developing a scheme that is both WB and ES. In [34], Waruszewski et al. devised an ES DG scheme for the rotating Euler equation

with gravity utilizing the first approach. However, their scheme does not account for the WB property and hence cannot capture isothermal equilibrium. In this work, we use the first approach as a foundation to develop a DG scheme for the Euler equations with gravity that preserves both ES and WB properties.

Furthermore, for the Euler equations, the density and pressure of the solution must remain positive to ensure well-posedness and prevent instability or simulation failure [40]. A numerical method that ensures positivity is known as a positivity-preserving (PP) scheme. In the pioneering work [40], Zhang and Shu proposed a simple high-order scaling-based PP DG method to solve the Euler equations. In [41], the technique is extended to the Euler equations with source terms. In the aforementioned works [35, 14], a similar approach is also applied to achieve the PP property for the Euler equations with gravity.

To our best knowledge, no DG scheme exists that is simultaneously WB, ES, and PP. In this work, we aim to develop a high-order structure-preserving nodal DG scheme that satisfies all these properties. Our contributions encompass the following aspects. Under the ES nodal DG framework, we propose a novel approach to modify the discretization of the source term to precisely match the form of entropy conservative fluxes, thereby ensuring exact balance for the numerical equilibrium state solution while preserving the ES property. Furthermore, we prove that the scheme is WB for arbitrary hydrostatic equilibrium states and both ES and PP for general states. A comprehensive suite of numerical experiments demonstrates the crucial role of each preserved property in our formulation. The numerical evidence indicates that omitting any single property leads to either computational breakdown or violations of critical physical laws in specific test configurations, highlighting the effectiveness of the proposed structure-preserving methodology.

The remainder of this paper is organized as follows. In Section 2, we introduce the Euler equations with gravity, together with their equilibrium solutions and entropy condition. Section 3 presents our structure-preserving nodal DG scheme for the one-dimensional (1D) case and its theoretical analysis. In Section 4, we extend this method to two dimensions (2D). In Section 5, various numerical examples are provided to demonstrate the performance of our proposed scheme. Section 6 concludes with a discussion of our results and potential directions for future work.

2 Euler Equations with Gravity

2.1 Governing Equations

In the general d -dimensional case ($d = 1, 2, 3$), the Euler equations with gravity can be expressed as the following nonlinear system of balance laws:

$$\mathbf{U}_t + \nabla \cdot \mathbf{F}(\mathbf{U}) = \mathbf{S}(\mathbf{U}, \mathbf{x}), \quad (\mathbf{x}, t) \in \mathbb{R}^d \times [0, +\infty), \quad (2.1)$$

where

$$\mathbf{U} = \begin{bmatrix} \rho \\ \rho \mathbf{u} \\ \mathcal{E} \end{bmatrix}, \quad \mathbf{F}(\mathbf{U}) = \begin{bmatrix} \rho \mathbf{u} \\ \rho \mathbf{u} \otimes \mathbf{u} + p I_d \\ \mathbf{u}(\mathcal{E} + p) \end{bmatrix}, \quad \mathbf{S}(\mathbf{U}, \mathbf{x}) = \begin{bmatrix} 0 \\ -\rho \nabla \phi \\ -\rho \mathbf{u} \cdot \nabla \phi \end{bmatrix}. \quad (2.2)$$

Here, ρ denotes the density, $\rho \mathbf{u}$ is the momentum, \mathcal{E} represents the total energy, I_d is the identity matrix, and p is the pressure. The source term \mathbf{S} models the gravitational force, where $\phi = \phi(\mathbf{x})$ denotes the gravitational potential and is time-independent. To close the system, the ideal gas equation of state is used:

$$\mathcal{E} = \frac{p}{\gamma - 1} + \frac{1}{2} \rho \|\mathbf{u}\|^2, \quad \text{with } \gamma = 1.4. \quad (2.3)$$

The density and pressure in the solution of (2.1) must remain positive for the well-posedness. That is we require $\mathbf{U}(\mathbf{x}, t) \in \mathcal{G}, \forall (\mathbf{x}, t) \in \mathbb{R}^d \times [0, +\infty)$, where \mathcal{G} denotes the *admissible set*

$$\mathcal{G} = \{(\rho, \rho \mathbf{u}, \mathcal{E}) : \rho > 0 \quad \text{and} \quad p(\rho, \rho \mathbf{u}, \mathcal{E}) > 0\}. \quad (2.4)$$

It can be verified that the set \mathcal{G} is convex when $\rho > 0$.

2.2 Steady-State Solutions

With the gravitational potential ϕ , the system (2.1) admits a set of time-independent solutions, called *equilibrium state solutions*, which satisfy

$$\nabla \cdot \mathbf{F}(\mathbf{U}) = \mathbf{S}(\mathbf{U}, \mathbf{x}).$$

For these solutions, the flux term is exactly balanced with the source term. In particular, in this work, we focus on the equilibrium state solutions with zero velocity, characterized by

$$\rho = \rho(\mathbf{x}), \quad \mathbf{u} = \mathbf{0}, \quad \nabla p = -\rho \nabla \phi, \quad (2.5)$$

referred to as the *hydrostatic equilibrium state* or *mechanical equilibrium state*. There are two important families of special steady-state solutions for (2.5). The first type is called the *isothermal hydrostatic equilibrium state*, in which the gas is assumed to obey the relation

$$p = \rho R T$$

with a constant temperature T . Here, R is the gas constant. Under this assumption, the solution of (2.5) is given by

$$\rho = \rho_0 \exp\left(-\frac{\phi}{RT_0}\right), \quad \mathbf{u} = \mathbf{0}, \quad p = p_0 \exp\left(-\frac{\phi}{RT_0}\right), \quad (2.6)$$

where ρ_0, p_0, T_0 are positive constants satisfying $p_0 = \rho_0 RT_0$. The second type is the *isentropic hydrostatic equilibrium state*, which assumes the entropy of the gas remains constant, i.e.,

$$p\rho^{-\gamma} = K_0.$$

Under this assumption, the solution of (2.5) is given by

$$\rho = \left(\frac{\gamma-1}{K_0\gamma}(C-\phi)\right)^{\frac{1}{\gamma-1}}, \quad \mathbf{u} = \mathbf{0}, \quad p = K_0\rho^\gamma, \quad (2.7)$$

where C and K_0 are constants.

2.3 Entropy Analysis

Consider a d -dimensional hyperbolic conservation law

$$\mathbf{U}_t + \nabla \cdot \mathbf{F}(\mathbf{U}) = \mathbf{0}, \quad \mathbf{F} = (\mathbf{F}_1, \dots, \mathbf{F}_d), \quad (2.8)$$

and suppose the state \mathbf{U} takes values in a convex set \mathcal{D} . A convex function $\mathcal{U}(\mathbf{U}) : \mathcal{D} \rightarrow \mathbb{R}$ is called an entropy function for system (2.8) if there exists an entropy flux $\mathcal{F}(\mathbf{U}) = (\mathcal{F}_1(\mathbf{U}), \dots, \mathcal{F}_d(\mathbf{U})) : \mathcal{D} \rightarrow \mathbb{R}^d$ such that

$$\mathcal{F}'_i(\mathbf{U}) = \mathcal{U}'(\mathbf{U}) \mathbf{F}'_i(\mathbf{U}), \quad i = 1, \dots, d. \quad (2.9)$$

Here, $\mathcal{F}'_i(\mathbf{U})$ and $\mathcal{U}'(\mathbf{U})$ are viewed as row vectors. The entropy function \mathcal{U} and the entropy flux \mathcal{F} together form an *entropy pair* $(\mathcal{U}, \mathcal{F})$. $\mathbf{V} = \mathcal{U}'(\mathbf{U})^T$ is called the *entropy variable*. If a system of conservation laws (2.8) admits an entropy pair, then left-multiplying by $\mathbf{V}(\mathbf{U})^T$ yields an additional entropy conservation law for smooth solutions

$$\mathcal{U}(\mathbf{U})_t + \nabla \cdot \mathcal{F}(\mathbf{U}) = 0. \quad (2.10)$$

For non-smooth solutions, the above equation is replaced by an inequality in the weak sense

$$\mathcal{U}(\mathbf{U})_t + \nabla \cdot \mathcal{F}(\mathbf{U}) \leq 0, \quad (2.11)$$

known as the *entropy condition*. In particular, a strictly convex function \mathcal{U} serves as an entropy function if and only if $\partial\mathbf{U}/\partial\mathbf{V}$ is a symmetric, positive-definite matrix and

$\partial \mathbf{F}_i(\mathbf{U}(\mathbf{V}))/\partial \mathbf{V}$ is symmetric for all i [18, 17]. In this case, there exist twice-differentiable scalar functions $\varphi(\mathbf{V})$ and $\psi_i(\mathbf{V})$, called the *potential function* and *potential flux*, with $\varphi(\mathbf{V})$ strictly convex, such that

$$\mathbf{U}(\mathbf{V})^T = \frac{\partial \varphi}{\partial \mathbf{V}}, \quad \mathbf{F}_i(\mathbf{V})^T = \frac{\partial \psi_i}{\partial \mathbf{V}}. \quad (2.12)$$

For the Euler equations without source term $\mathbf{S}(\mathbf{U}, \mathbf{x})$, Harten [21] showed that there exists a family of entropy pairs related to the physical specific entropy $s = \ln(p\rho^{-\gamma})$, satisfying the symmetrization condition. However, to symmetrize the viscous term in the compressible Navier-Stokes equations with heat conduction [22], there is only one choice of the entropy pair

$$\mathcal{U} = -\frac{\rho s}{\gamma - 1}, \quad \mathcal{F} = -\frac{\rho s}{\gamma - 1} \mathbf{u}. \quad (2.13)$$

Correspondingly,

$$\mathbf{V} = \mathcal{U}'(\mathbf{U})^T = \begin{bmatrix} \frac{\gamma - s}{\gamma - 1} - \frac{\rho \|\mathbf{u}\|^2}{2p} \\ \rho \mathbf{u}/p \\ -\rho/p \end{bmatrix},$$

and $\varphi = \rho$, $\psi_i = \rho u_i$. Notice that

$$\mathbf{V}(\mathbf{U})^T \mathbf{S}(\mathbf{U}, \mathbf{x}) = -\rho \nabla \phi \cdot \frac{\rho \mathbf{u}}{p} - (-\rho \mathbf{u} \cdot \nabla \phi) \frac{\rho}{p} = 0,$$

and hence, it is straightforward to verify that the Euler equations with gravity (2.1) also satisfy the entropy inequality (2.11) with the entropy pair (2.13) [13]. This observation is critical to design a scheme that is ES and WB simultaneously.

3 Structure-Preserving Nodal DG Method in One Dimension

In this section, we formulate the proposed scheme for the 1D case of (2.1), which is given as

$$\begin{bmatrix} \rho \\ m \\ \mathcal{E} \end{bmatrix}_t + \begin{bmatrix} m \\ \rho u^2 + p \\ u(\mathcal{E} + p) \end{bmatrix}_x = \begin{bmatrix} 0 \\ -\rho \phi_x \\ -m \phi_x \end{bmatrix}, \quad (3.14)$$

where $m = \rho u$ is the momentum. Denote such a system by

$$\mathbf{U}_t + \mathbf{F}(\mathbf{U})_x = \mathbf{S}(\mathbf{U}, x)$$

with $\mathbf{F} = (F_1, F_2, F_3)^T$.

Assume that the 1D spatial domain $\Omega = [a, b]$ is divided into N uniform cells $\mathcal{K} = \{K_i = [x_{i-1/2}, x_{i+1/2}], i = 1, \dots, N\}$ with $x_{1/2} = a$, $x_{N+1/2} = b$ and mesh size $\Delta x = x_{i+1/2} - x_{i-1/2}$. Define the finite element space as the piecewise polynomial space of degree at most k :

$$V_h^k = \{w(x) : w(x)|_{K_i} \in P^k(K_i), \quad \forall K_i \in \mathcal{K}\}.$$

The classic semi-discrete DG scheme for (3.14) is: Find $\mathbf{U}_h \in [V_h^k]^3$, such that for any test function $\mathbf{W} \in [V_h^k]^3$ and cell $K_i \in \mathcal{K}$,

$$\int_{K_i} \frac{\partial \mathbf{U}_h}{\partial t} \cdot \mathbf{W} \, dx = \int_{K_i} \mathbf{F}(\mathbf{U}_h) \cdot \frac{\partial \mathbf{W}}{\partial x} \, dx - \hat{\mathbf{F}}_{i+1/2}^- \mathbf{W}_{i+1/2}^- + \hat{\mathbf{F}}_{i-1/2}^+ \mathbf{W}_{i-1/2}^+ + \int_{K_i} \mathbf{S} \cdot \mathbf{W} \, dx. \quad (3.15)$$

Here, $\hat{\mathbf{F}}_{i+1/2}$ represents the numerical flux at the cell interface $x_{i+1/2}$. In this work, we employ the Lax-Friedrichs flux:

$$\hat{\mathbf{F}}^{LF}(\mathbf{U}_L, \mathbf{U}_R) = \frac{1}{2}(\mathbf{F}(\mathbf{U}_R) + \mathbf{F}(\mathbf{U}_L)) - \frac{\alpha}{2}(\mathbf{U}_R - \mathbf{U}_L), \quad (3.16)$$

where α is an estimate of the maximum local wave speed and will be determined below.

3.1 Gauss-Lobatto Quadrature and the SBP Property

We now apply the Gauss-Lobatto quadrature rule with $k + 1$ quadrature points to build the nodal DG scheme. Let

$$-1 = X_0 < X_1 < \dots < X_k = 1,$$

denote the Gauss-Lobatto quadrature points on the reference element $I = [-1, 1]$, with corresponding quadrature weights $\{\omega_l\}_{l=0}^k$. The difference matrix D is defined as $D_{jl} = L'_l(X_j)$, where L_l is the l -th Lagrange basis polynomial satisfying $L_l(X_j) = \delta_{lj}$. The mass matrix M and stiffness matrix S are given by $M = \text{diag}\{\omega_0, \omega_1, \dots, \omega_k\}$ and $S = MD$. We recall the following properties of these matrices [7]:

Lemma 3.1. *Let the boundary matrix B be defined as*

$$B = \text{diag}\{-1, 0, 0, \dots, 0, 0, 1\} =: \text{diag}\{\tau_0, \dots, \tau_k\},$$

then $S + S^T = B$.

Lemma 3.2. For each $0 \leq j \leq k$, we have

$$\sum_{l=0}^k D_{jl} = \sum_{l=0}^k S_{jl} = 0, \quad \sum_{l=0}^k S_{lj} = \tau_j.$$

Using the matrices defined above, we can construct the original nodal DG scheme in a compact matrix-vector formulation based on the nodal values. First, we introduce the following shorthand notation:

$$x_i(X) = x_i + \frac{\Delta x}{2} X, \quad \mathbf{U}_{i_1}^i = \mathbf{U}_h(x_i(X_{i_1})), \quad \mathbf{F}_{i_1}^i = \mathbf{F}(\mathbf{U}_{i_1}^i), \quad (3.17)$$

$$\mathbf{F}_{i_1}^{*,i} = \begin{cases} \hat{\mathbf{F}}_{i-1/2} =: \hat{\mathbf{F}}(\mathbf{U}_k^{i-1}, \mathbf{U}_0^i), & i_1 = 0, \\ 0, & 0 < i_1 < k, \\ \hat{\mathbf{F}}_{i+1/2} =: \hat{\mathbf{F}}(\mathbf{U}_k^i, \mathbf{U}_0^{i+1}), & i_1 = k. \end{cases} \quad (3.18)$$

Then the solution is represented by

$$\mathbf{U}_h(x)|_{K_i} = \sum_{i_1=0}^k \mathbf{U}_{i_1}^i L_{i_1} \left(\frac{x - x_i}{\Delta x/2} \right). \quad (3.19)$$

Then, after applying Gauss-Lobatto quadrature and the SBP properties in Lemma 3.1, (3.15) transforms into a nodal DG scheme, with the strong formulation given by

$$\frac{\Delta x}{2} \frac{d\mathbf{U}_{i_1}^i}{dt} + \sum_{l=0}^k D_{i_1,l} \mathbf{F}_l^i + \frac{\tau_{i_1}}{\omega_{i_1}} (\mathbf{F}_{i_1}^{*,i} - \mathbf{F}_{i_1}^i) = \frac{\Delta x}{2} \mathbf{S}(\mathbf{U}_{i_1}^i, x_i(X_{i_1})) \quad (3.20)$$

for $i = 1, \dots, N$, $i_1 = 0, \dots, k$. Meanwhile, it is known that the nodal DG scheme above may fail to preserve physical structures of interest. In this work, we systematically modify this formulation to ensure that the resulting scheme simultaneously preserves the following properties:

1. **Well-balanced (WB) property:** If the initial condition is a steady-state solution $\mathbf{U}^e(x) = (\rho^e(x), 0, \mathcal{E}^e(x))^T$, the numerical solution remains $\mathbf{U}_h = \mathbf{U}_h^e$, where \mathbf{U}_h^e denotes the interpolating polynomial of \mathbf{U}^e at Gauss-Lobatto points.
2. **Entropy-stable (ES) property:** Under the assumption of periodic, compactly

supported, or reflective boundary conditions, the semi-discrete scheme satisfies

$$\frac{d}{dt} \left(\sum_{i=1}^N \sum_{i_1=0}^k \frac{\Delta x}{2} \omega_{i_1} \mathcal{U}(\mathbf{U}_{i_1}^i) \right) \leq 0.$$

3. **Positivity-preserving (PP) property:** if the numerical solution at time t^n satisfies $\mathbf{U}_{i_1}^{i,n} \in \mathcal{G}$, then the updated solution at t^{n+1} satisfies

$$\mathbf{U}_{i_1}^{i,n+1} \in \mathcal{G} \quad \text{for any } i \text{ and } i_1.$$

3.2 Proposed scheme

For a given steady state \mathbf{U}^e that satisfies (2.5), we have the following relations:

$$-\rho\phi_x = -\frac{\rho}{\rho^e}\rho^e\phi_x = \frac{\rho}{\rho^e}p_x^e, \quad -m\phi_x = -\frac{m}{\rho^e}\rho^e\phi_x = \frac{m}{\rho^e}p_x^e.$$

Hence, following the approach in [25, 35, 14], we rewrite the momentum and energy equations as

$$\frac{\partial m}{\partial t} + \frac{\partial(\rho u^2 + p)}{\partial x} = \frac{\rho}{\rho^e} \frac{\partial p^e}{\partial x}, \quad \frac{\partial \mathcal{E}}{\partial t} + \frac{\partial(u(\mathcal{E} + p))}{\partial x} = \frac{m}{\rho^e} \frac{\partial p^e}{\partial x}, \quad (3.21)$$

which facilitates the design of discretization for the source term that precisely matches the flux term in the equilibrium state solution. By utilizing the entropy conservative fluxes [7] and the fact that $p^e = F_2(\mathbf{U}^e)$, the proposed nodal DG scheme is given by

$$\frac{\Delta x}{2} \frac{d\mathbf{U}_{i_1}^i}{dt} + \sum_{l=0}^k 2D_{i_1,l} \mathbf{F}^S(\mathbf{U}_{i_1}^i, \mathbf{U}_l^i) + \frac{\tau_{i_1}}{\omega_{i_1}} (\mathbf{F}_{i_1}^{*,i} - \mathbf{F}_{i_1}^i) = \mathbf{S}_{i_1}^i, \quad (3.22)$$

where $\mathbf{F}_{i_1}^{*,i}$ is given in (3.18), and

$$\mathbf{S}_{i_1}^i = (0, \rho_{i_1}^i \Theta_{i_1}^i, m_{i_1}^i \Theta_{i_1}^i)^T \quad (3.23)$$

is a high-order approximation to the source term with

$$\Theta_{i_1}^i := \frac{1}{\rho_{i_1}^{e,i}} \sum_{l=0}^k 2D_{i_1,l} F_2^S(\mathbf{U}_{i_1}^{e,i}, \mathbf{U}_l^{e,i}) = \frac{1}{\rho_{i_1}^{e,i}} (p_x^e)_{i_1}^i \frac{\Delta x}{2} + \mathcal{O}(\Delta x^{k+1}). \quad (3.24)$$

In addition, $\mathbf{F}^S = (F_1^S, F_2^S, F_3^S)^T$ denotes an entropy conservative flux, and $\hat{\mathbf{F}} = (\hat{F}_1, \hat{F}_2, \hat{F}_3)^T$ used in (3.18) denotes an entropy stable flux, each with specific definitions given below.

Definition 3.1. A consistent, symmetric two-point numerical flux $\mathbf{F}^S(\mathbf{U}_L, \mathbf{U}_R)$ is said to be entropy conservative, if for the given entropy function \mathcal{U} ,

$$(\mathbf{V}_R - \mathbf{V}_L)^T \mathbf{F}^S(\mathbf{U}_L, \mathbf{U}_R) = (\psi_R - \psi_L). \quad (3.25)$$

Definition 3.2. A consistent two-point numerical flux $\hat{\mathbf{F}}(\mathbf{U}_L, \mathbf{U}_R)$ is said to be entropy stable, if for the given entropy function \mathcal{U} ,

$$(\mathbf{V}_R - \mathbf{V}_L)^T \hat{\mathbf{F}}(\mathbf{U}_L, \mathbf{U}_R) \leq (\psi_R - \psi_L).$$

For the Euler equations, Chandrashekar [4] proposed the following entropy conservative flux:

$$\begin{aligned} F_1^S &= \hat{\rho}\bar{u}, \\ F_2^S &= \frac{\bar{p}}{2\hat{\beta}} + \bar{u}F_1^S, \\ F_3^S &= \left(\frac{1}{2(\gamma-1)\hat{\beta}} - \frac{1}{2}\bar{u}^2 \right) F_1^S + \bar{u}F_2^S, \end{aligned}$$

where $\beta = \rho/2p$, and

$$\bar{\alpha} = \frac{\alpha_l + \alpha_r}{2}, \quad \hat{\alpha} = \frac{\alpha_r - \alpha_l}{\ln \alpha_r - \ln \alpha_l}.$$

For entropy stable fluxes, in [33] Toro suggests the two-rarefaction approximation, and in [20] Guermond and Popov demonstrated that the two-rarefaction approximated wave speeds can achieve entropy stability for the Euler equations with $1 < \gamma \leq 5/3$ when using the Lax-Friedrichs flux. Therefore, we set the value of α in the Lax-Friedrichs flux (3.16) as

$$\alpha = \max \{ |u_L| + c_L, |u_R| + c_R, \alpha^{RRF}(\mathbf{U}_L, \mathbf{U}_R) \}$$

to ensure entropy stability, where $c = \sqrt{\gamma p/\rho}$, and α^{RRF} is determined using the two-rarefaction approximation technique.

The semi-discrete nodal DG scheme (3.22) can be presented as an ODE system

$$\frac{d\mathbf{U}_h}{dt} = \mathcal{L}_h(\mathbf{U}_h).$$

The fully-discrete scheme is obtained by applying a strong stability preserving Runge-Kutta (SSP-RK) method to solve this ODE system. To further ensure the PP property, we propose to incorporate the well-established PP limiter [40]. Since an SSP-RK method is a convex combination of forward Euler steps, we focus on the fully-discrete scheme with forward Euler time discretization, which is given by

$$\mathbf{U}_h^{EF} = \mathbf{U}_h^n + \Delta t \cdot \mathcal{L}_h(\mathbf{U}_h^n). \quad (3.26)$$

The high order scaling-based PP limiter, denoted by Π_h , is applied to guarantee the positivity of the density and pressure at each Gauss–Lobatto point,

$$\mathbf{U}_h^{n+1} = \Pi_h \mathbf{U}_h^{EF} = \Pi_h (\mathbf{U}_h^n + \Delta t \cdot \mathcal{L}_h(\mathbf{U}_h^n)). \quad (3.27)$$

In particular, Π_h scales the numerical solutions towards the cell averages in K_i using two parameters $\theta_i^{(1)}, \theta_i^{(2)} \in [0, 1]$, as defined by

$$\begin{aligned} \tilde{\rho}_{i_1}^{i,EF} &= (1 - \theta_i^{(1)}) \bar{\rho}^{i,EF} + \theta_i^{(1)} \rho_{i_1}^{i,EF}, \\ \begin{pmatrix} \rho_{i_1} \\ m_{i_1} \\ \mathcal{E}_{i_1} \end{pmatrix}^{i,n+1} &= (1 - \theta_i^{(2)}) \begin{pmatrix} \bar{\rho} \\ \bar{m} \\ \bar{\mathcal{E}} \end{pmatrix}^{i,EF} + \theta_i^{(2)} \begin{pmatrix} \tilde{\rho}_{i_1} \\ m_{i_1} \\ \mathcal{E}_{i_1} \end{pmatrix}^{i,EF}. \end{aligned} \quad (3.28)$$

Here,

$$\bar{\mathbf{U}}^{i,EF} = \frac{1}{\Delta x} \int_{K_i} \mathbf{U}_h^{EF}(x) dx = \sum_{i_1=0}^k \frac{\omega_{i_1}}{2} \mathbf{U}_{i_1}^{i,EF}$$

is the cell average of \mathbf{U}_h^{EF} in K_i . The value of θ is computed as

$$\theta_i^{(1)} = \min \left\{ \frac{\bar{\rho}^{i,EF} - \varepsilon}{\bar{\rho}^{i,EF} - \rho_m}, 1 \right\}, \quad \rho_m = \min_{0 \leq i_1 \leq k} \rho_{i_1}^{i,EF}, \quad (3.29)$$

$$\theta_i^{(2)} = \min_{0 \leq i_1 \leq k} \{t_{i_1}\}, \quad t_{i_1} = \begin{cases} 1, & p(\tilde{\mathbf{U}}_{i_1}^{i,EF}) \geq \varepsilon, \\ \tilde{t}_{i_1}, & p(\tilde{\mathbf{U}}_{i_1}^{i,EF}) < \varepsilon. \end{cases} \quad (3.30)$$

Here, the parameter ε is a small number, and we set $\varepsilon = 10^{-13}$ as suggested in [40]. In (3.30), $\tilde{\mathbf{U}}_{i_1}^{i,EF} = (\tilde{\rho}_{i_1}^{i,EF}, m_{i_1}^{i,EF}, \mathcal{E}_{i_1}^{i,EF})^T$, and the scaling factor \tilde{t}_{i_1} is solved from the nonlinear equation

$$p\left((1 - \tilde{t}_{i_1})\bar{\mathbf{U}}^{i,n} + \tilde{t}_{i_1}\tilde{\mathbf{U}}_{i_1}^{i,n}\right) = \varepsilon.$$

In particular, if $\mathbf{U}_{i_1}^{i,EF} \in \mathcal{G}$ for all i_1 , then $\theta_i^{(1)} = \theta_i^{(2)} = 1$. It should be noted that Π_h does not change the cell average, i.e. $\bar{\mathbf{U}}^{i,n+1} = \bar{\mathbf{U}}^{i,EF}$. Moreover, if $\bar{\mathbf{U}}^{i,EF} \in \mathcal{G}$, the limiter (3.28) ensures the nodal value at each Gauss-Lobatto point $\mathbf{U}_{i_1}^{i,n+1} \in \mathcal{G}$.

3.3 Properties of the scheme

In this subsection, we prove that the scheme (3.22) is WB, ES, and the fully-discrete scheme (3.27) is PP under a suitable CFL condition.

3.3.1 Well-balanced property

Theorem 3.1 (Well-balancedness). *The scheme (3.22) is WB for a general known stationary hydrostatic solution $\mathbf{U}^e = (\rho^e, 0, \mathcal{E}^e)$, i.e.*

$$\mathcal{L}_h(\mathbf{U}_h) = \mathbf{0}, \quad \text{if } \mathbf{U}_h = \mathbf{U}_h^e. \quad (3.31)$$

Proof. As $\mathbf{U}_h = \mathbf{U}_h^e$, we have $\mathbf{U}_{i_1}^i = \mathbf{U}_{i_1}^{e,i}$. It is easy to verify

$$F_1 = F_1^S = \hat{F}_1 = 0, \quad F_3 = F_3^S = \hat{F}_3 = 0, \quad (3.32)$$

thus $\mathcal{L}_{h,1}(\mathbf{U}_h)|_{i_1}^i = \mathcal{L}_{h,3}(\mathbf{U}_h)|_{i_1}^i = 0$. For the equation of momentum, we note that \mathbf{U}_h^e is continuous at the interfaces $x_{i+1/2}$, since it interpolates the steady state solution \mathbf{U}^e at Gauss-Lobatto points, which include the interface location. Utilizing the consistency of $\hat{\mathbf{F}}$, we have

$$F_{2,i_1}^i = p_{i_1}^{e,i}, \quad \hat{F}_{2,i+1/2} = p^e(x_{i+1/2}) = F_{2,k}^i = F_{2,0}^{i+1}.$$

Therefore,

$$\begin{aligned} \mathcal{L}_{h,2}(\mathbf{U}_h)|_{i_1}^i &= - \sum_{l=0}^k 2D_{i_1,l} F_2^S(\mathbf{U}_{i_1}^i, \mathbf{U}_l^i) - \frac{\tau_{i_1}}{\omega_{i_1}} (F_{2,i_1}^{*,i} - F_{2,i_1}^i) \\ &\quad + \frac{\rho_{i_1}^i}{\rho_{i_1}^{e,i}} \sum_{l=0}^k 2D_{i_1,l} F_2^S(\mathbf{U}_{i_1}^{e,i}, \mathbf{U}_l^{e,i}) \\ &= - \sum_{l=0}^k 2D_{i_1,l} F_2^S(\mathbf{U}_{i_1}^{e,i}, \mathbf{U}_l^{e,i}) - 0 + 1 \sum_{l=0}^k 2D_{i_1,l} F_2^S(\mathbf{U}_{i_1}^{e,i}, \mathbf{U}_l^{e,i}) = 0. \end{aligned}$$

Hence, $\mathcal{L}_h(\mathbf{U}_h) = \mathbf{0}$. □

Remark 3.1. *The proof of Theorem 3.1 shows the necessity of choosing the numerical equilibrium state as the Gauss-Lobatto interpolating polynomial. For alternative approximations, \hat{F}_1 and \hat{F}_3 in (3.32) may be nonzero due to possible discontinuities at interfaces. In [14], the authors proposed a specialized choice of α for the Lax-Friedrichs flux, where α vanishes when the solution \mathbf{U}_h coincides with the numerical equilibrium state \mathbf{U}_h^e , ensuring $\hat{F}_1 = \hat{F}_3 = 0$. However, the modified Lax-Friedrichs flux is not entropy stable according to the definition 3.2, which requires α to be sufficiently large [20, 7].*

Remark 3.2. *For the fully-discrete scheme (3.27), if $\mathbf{U}_h^n = \mathbf{U}_h^e$, then $\mathcal{L}_h(\mathbf{U}_h^n) = \mathbf{0}$, yielding $\mathbf{U}_h^{EF} = \mathbf{U}_h^e$. When $\mathbf{U}^e(x) \in \mathcal{G}$, we have*

$$\mathbf{U}_{i_1}^{EF,i} = \mathbf{U}^e(x_i(X_{i_1})) \in \mathcal{G}$$

for all i, i_1 , resulting in $\theta_i^{(1)} = \theta_i^{(2)} = 1$. Therefore, we have $\mathbf{U}_h^{n+1} = \Pi_h(\mathbf{U}_h^{EF}) = \mathbf{U}_h^e$, i.e., the fully-discrete scheme is WB.

3.3.2 Entropy-stable property

Theorem 3.2 (Entropy stability). *Assume that the boundary is periodic, compact support, or reflective. Then, the semi-discrete scheme (3.22) is entropy conservative within each cell in the sense of*

$$\frac{d}{dt} \left(\sum_{i_1=0}^k \frac{\Delta x}{2} \omega_{i_1} \mathcal{U}(\mathbf{U}_{i_1}^i) \right) = \mathcal{F}_0^{*,i} - \mathcal{F}_k^{*,i}, \quad (3.33)$$

and ES in the sense of

$$\frac{d}{dt} \mathcal{U}^{tot}(\mathbf{U}_h) = \frac{d}{dt} \left(\sum_{i=1}^N \sum_{i_1=0}^k \frac{\Delta x}{2} \omega_{i_1} \mathcal{U}(\mathbf{U}_{i_1}^i) \right) \leq 0, \quad (3.34)$$

where

$$\mathcal{F}_k^{*,i} = (\mathbf{V}_k^i)^T \hat{\mathbf{F}}_{i+1/2} - \psi_k^i, \quad \mathcal{F}_0^{*,i} = (\mathbf{V}_0^i)^T \hat{\mathbf{F}}_{i-1/2} - \psi_0^i.$$

Proof. Left multiplying (3.22) by \mathbf{V}^T and integral in cell K_i yields

$$\begin{aligned} \sum_{i_1=0}^k \frac{\omega_{i_1} \Delta x}{2} \frac{d\mathcal{U}(\mathbf{U}_{i_1}^i)}{dt} &= \sum_{i_1=0}^k \frac{\omega_{i_1} \Delta x}{2} (\mathbf{V}_{i_1}^i)^T \frac{d\mathbf{U}_{i_1}^i}{dt} \\ &= - \sum_{i_1=0}^k \sum_{l=0}^k 2S_{i_1,l} (\mathbf{V}_{i_1}^i)^T \mathbf{F}^S(\mathbf{U}_{i_1}^i, \mathbf{U}_l^i) - \sum_{i_1=0}^k \tau_{i_1} (\mathbf{V}_{i_1}^i)^T (\mathbf{F}_{i_1}^{*,i} - \mathbf{F}_{i_1}^i) \\ &\quad + \sum_{i_1=0}^k \frac{\omega_{i_1}}{2} (\mathbf{V}_{i_1}^i)^T \mathbf{S}_{i_1}^i \\ &=: -T_1 - T_2 + T_3. \end{aligned}$$

For T_1 , [7] has proved that

$$\sum_{i_1=0}^k \sum_{l=0}^k 2S_{i_1,l} (\mathbf{V}_{i_1}^i)^T \mathbf{F}^S(\mathbf{U}_{i_1}^i, \mathbf{U}_l^i) = \sum_{i_1=0}^k \tau_{i_1} \left((\mathbf{V}_{i_1}^i)^T \mathbf{F}_{i_1}^i - \psi_{i_1}^i \right).$$

Hence $-T_1 - T_2 = -(\mathcal{F}_k^{*,i} - \mathcal{F}_0^{*,i})$. On the other hand, we have

$$(\mathbf{V}_{i_1}^i)^T \mathbf{S}_{i_1}^i = \left(\frac{m_{i_1}^i}{p_{i_1}^i} \right) (\rho_{i_1}^i \Theta_{i_1}^i) - \left(\frac{\rho_{i_1}^i}{p_{i_1}^i} \right) (m_{i_1}^i \Theta_{i_1}^i) = 0,$$

which implies $T_3 = 0$. Thus, we have proved (3.33).

Moreover, for an entropy stable flux $\hat{\mathbf{F}}$, [7] demonstrated that the following inequality

holds at each cell interface:

$$-(\mathcal{F}_k^{*,i} - \mathcal{F}_0^{*,i+1}) = (\psi_k^i - \psi_0^{i+1}) - (\mathbf{V}_k^i - \mathbf{V}_0^{i+1})^T \hat{\mathbf{F}}_{i+1/2} \leq 0.$$

Hence, summing (3.33) over i yields (3.34). \square

Remark 3.3. Most existing WB schemes [25, 6, 14] only modify the discretization of the second component of source term \mathbf{S} , because the third component is automatically zero for a steady state solution. But in our proposed scheme, to further satisfy the entropy condition, it is also necessary to modify the discretization of the third component of \mathbf{S} to ensure $T_3 = 0$.

Remark 3.4. It has been proved in [7] that the PP limiter Π_h (3.28) will not increase the “total entropy” in each cell, i.e.,

$$\sum_{i_1=0}^k \omega_{i_1} \mathcal{U}((\Pi_h \mathbf{U}_h)_{i_1}^i) \leq \sum_{i_1=0}^k \omega_{i_1} \mathcal{U}(\mathbf{U}_{i_1}^i). \quad (3.35)$$

Hence, if a fully discrete scheme of (3.22) is ES, then the scheme incorporating the PP limiter remains ES as well.

3.3.3 Positivity-preserving property

Theorem 3.3 (Positivity-preserving). Assume $\mathbf{U}_{i_1}^{i,n} \in \mathcal{G}$ for all i, i_1 . Then, the solution of the fully-discrete scheme (3.27) satisfies $\bar{\mathbf{U}}^{i,n+1} \in \mathcal{G}$ under the time step restriction

$$\lambda = \frac{\Delta t}{\Delta x} < \min \left\{ \frac{\omega_0}{4\alpha_0}, \min_{i,i_1} \left\{ \frac{1}{4|\Theta_{i_1}^i|} \sqrt{\frac{1}{(\gamma-1)\beta_{i_1}^i}} \right\} \right\}, \quad \alpha_0 = \max_{\Omega} \{|u| + c\}. \quad (3.36)$$

Proof. Utilizing the definition (3.28), the PP limiter Π_h does not change the cell average, i.e. $\bar{\mathbf{U}}^{i,n+1} = \bar{\mathbf{U}}^{i,EF}$. Thus, from (3.27), we can obtain the equation for cell averages

$$\Delta x \frac{\bar{\mathbf{U}}^{i,n+1} - \bar{\mathbf{U}}^{i,n}}{\Delta t} = -\hat{\mathbf{F}}_{i+1/2} + \hat{\mathbf{F}}_{i-1/2} + \sum_{i_1=0}^k \omega_{i_1} \mathbf{S}_{i_1}^i.$$

Following the approach in [41], we derive the following:

$$\begin{aligned} \bar{\mathbf{U}}^{i,n+1} &= \sum_{i_1=0}^k \frac{\omega_{i_1}}{2} \mathbf{U}_{i_1}^{i,n} - \lambda \left[\hat{\mathbf{F}}(\mathbf{U}_k^{i,n}, \mathbf{U}_0^{i+1,n}) - \hat{\mathbf{F}}(\mathbf{U}_k^{i-1,n}, \mathbf{U}_0^{i,n}) \right] + \lambda \sum_{i_1=0}^k \omega_{i_1} \mathbf{S}_{i_1}^i \\ &= \frac{\omega_0}{4} \mathbf{U}_0^{i,n} - \lambda \left[\hat{\mathbf{F}}(\mathbf{U}_0^{i,n}, \mathbf{U}_k^{i,n}) - \hat{\mathbf{F}}(\mathbf{U}_k^{i-1,n}, \mathbf{U}_0^{i,n}) \right] \\ &\quad + \frac{\omega_k}{4} \mathbf{U}_k^{i,n} - \lambda \left[\hat{\mathbf{F}}(\mathbf{U}_k^{i,n}, \mathbf{U}_0^{i+1,n}) - \hat{\mathbf{F}}(\mathbf{U}_0^{i,n}, \mathbf{U}_k^{i,n}) \right] \end{aligned}$$

$$\begin{aligned}
& + \frac{1}{2} \sum_{i_1=1}^{k-1} \frac{\omega_{i_1}}{2} \mathbf{U}_{i_1}^{i,n} + \frac{1}{2} \sum_{i_1=0}^k \frac{\omega_{i_1}}{2} \mathbf{U}_{i_1}^{i,n} + \lambda \sum_{i_1=0}^k \omega_{i_1} \mathbf{S}_{i_1}^i \\
& = \frac{\omega_0}{4} \mathbf{H}_0 + \frac{\omega_k}{4} \mathbf{H}_k + \sum_{i_1=1}^{k-1} \frac{\omega_{i_1}}{4} \mathbf{U}_{i_1}^{i,n} + \sum_{i_1=0}^k \frac{\omega_{i_1}}{4} (\mathbf{U}_{i_1}^{i,n} + 4\lambda \mathbf{S}_{i_1}^i),
\end{aligned}$$

which is a convex combination of \mathbf{H}_0 , \mathbf{H}_k , $\{\mathbf{U}_{i_1}^{i,n}\}_{i_1=1}^{k-1}$, $\{\mathbf{U}_{i_1}^{i,n} + 4\lambda \mathbf{S}_{i_1}^i\}_{i_1=0}^k$ as $\sum_{i_1=0}^k \omega_{i_1} = 2$.

Here

$$\begin{aligned}
\mathbf{H}_0 & = \mathbf{U}_0^{i,n} - \frac{4\lambda}{\omega_0} \left[\hat{\mathbf{F}}(\mathbf{U}_0^{i,n}, \mathbf{U}_k^{i,n}) - \hat{\mathbf{F}}(\mathbf{U}_k^{i-1,n}, \mathbf{U}_0^{i,n}) \right], \\
\mathbf{H}_k & = \mathbf{U}_k^{i,n} - \frac{4\lambda}{\omega_k} \left[\hat{\mathbf{F}}(\mathbf{U}_k^{i,n}, \mathbf{U}_0^{i+1,n}) - \hat{\mathbf{F}}(\mathbf{U}_0^{i,n}, \mathbf{U}_k^{i,n}) \right].
\end{aligned}$$

Given the convexity of \mathcal{G} , if we have

$$\mathbf{H}_0 \in \mathcal{G}, \quad \mathbf{H}_k \in \mathcal{G}, \quad \mathbf{U}_{i_1}^{i,n} + 4\lambda \mathbf{S}_{i_1}^i \in \mathcal{G}, \quad (3.37)$$

then $\bar{\mathbf{U}}^{i,n+1} \in \mathcal{G}$. In [41], it is proved that $\mathbf{H}_0, \mathbf{H}_k \in \mathcal{G}$ when $4\lambda\alpha_0/\omega_0 \leq 1$. On the other hand, given (3.23), we have

$$\mathbf{U}_{i_1}^{i,n} + 4\lambda \mathbf{S}_{i_1}^i = \begin{bmatrix} \rho_{i_1}^{i,n} \\ m_{i_1}^{i,n} + 4\lambda \rho_{i_1}^{i,n} \Theta_{i_1}^i \\ \mathcal{E}_{i_1}^{i,n} + 4\lambda m_{i_1}^{i,n} \Theta_{i_1}^i \end{bmatrix} =: \mathbf{U}^*.$$

Evidently, the density of state \mathbf{U}^* is $\rho_{i_1}^{i,n}$ and is therefore positive. Then, $\mathbf{U}^* \in \mathcal{G}$ if and only if

$$\mathcal{E}_{i_1}^{i,n} + 4\lambda m_{i_1}^{i,n} \Theta_{i_1}^i - \frac{(m_{i_1}^{i,n} + 4\lambda \rho_{i_1}^{i,n} \Theta_{i_1}^i)^2}{2\rho_{i_1}^{i,n}} > 0. \quad (3.38)$$

Solving the inequality (3.38) yields

$$\lambda < \frac{1}{4|\Theta_{i_1}^i|} \sqrt{\frac{1}{(\gamma-1)\beta_{i_1}^i}},$$

which is the condition for λ in (3.36). Thus, the proof is complete. \square

Remark 3.5. Under the restriction (3.36), we apply the limiter Π_h after each forward Euler step, which will enforce the nodal values satisfying $\mathbf{U}_{i_1}^{i,n+1} \in \mathcal{G}$ at Gauss-Lobatto points.

4 Structure-preserving nodal DG method in two dimensions

The 2D Euler equations with gravity are expressed as

$$\begin{bmatrix} \rho \\ m \\ n \\ \mathcal{E} \end{bmatrix}_t + \begin{bmatrix} m \\ \rho u^2 + p \\ \rho uv \\ u(\mathcal{E} + p) \end{bmatrix}_x + \begin{bmatrix} n \\ \rho uv \\ \rho v^2 + p \\ v(\mathcal{E} + p) \end{bmatrix}_y = \begin{bmatrix} 0 \\ -\rho\phi_x \\ -\rho\phi_y \\ -m\phi_x - n\phi_y \end{bmatrix}, \quad (4.39)$$

with $m = \rho u$, $n = \rho v$, and are denoted by

$$\mathbf{U}_t + \mathbf{F}(\mathbf{U})_x + \mathbf{G}(\mathbf{U})_y = \mathbf{S}(\mathbf{U}, x, y).$$

The corresponding entropy fluxes \mathcal{F}_1 , \mathcal{F}_2 in (2.9) are denoted by \mathcal{F} , \mathcal{G} , and the potential fluxes ψ_1 , ψ_2 in (2.12) are denoted by ψ_F , ψ_G . Assume that the 2D spatial domain $\Omega = [a, b] \times [c, d]$ is divided into an $N_x \times N_y$ uniform rectangular mesh with cells $\mathcal{K} = \{K_{ij} = [x_{i-1/2}, x_{i+1/2}] \times [y_{j-1/2}, y_{j+1/2}]\}$. The mesh sizes in x and y directions are denoted by Δx and Δy , respectively, where $\Delta x = x_{i+1/2} - x_{i-1/2}$ and $\Delta y = y_{j+1/2} - y_{j-1/2}$.

4.1 Proposed scheme

For a given stationary steady state $\mathbf{U}^e(x)$ of (4.39), we have

$$-\rho\phi_x = -\frac{\rho}{\rho^e}\rho^e\phi_x = \frac{\rho}{\rho^e}p_x^e, \quad -m\phi_x = -\frac{m}{\rho^e}\rho^e\phi_x = \frac{m}{\rho^e}p_x^e, \quad -n\phi_y = -\frac{n}{\rho^e}\rho^e\phi_y = \frac{n}{\rho^e}p_y^e,$$

and $p^e = F_2(\mathbf{U}^e) = G_3(\mathbf{U}^e)$. We introduce the following shorthand notation

$$x_i(X) = x_i + \frac{\Delta x}{2}X, \quad y_j(Y) = y_j + \frac{\Delta y}{2}Y,$$

$$\mathbf{U}_{i_1, j_1}^{i, j} = \mathbf{U}_h(x_i(X_{i_1}), y_j(Y_{j_1})), \quad \mathbf{F}_{i_1, j_1}^{i, j} = \mathbf{F}(\mathbf{U}_{i_1, j_1}^{i, j}), \quad \mathbf{G}_{i_1, j_1}^{i, j} = \mathbf{G}(\mathbf{U}_{i_1, j_1}^{i, j}),$$

$$\mathbf{F}_{i_1, j_1}^{*, i, j} = \begin{cases} \hat{\mathbf{F}}(\mathbf{U}_{k, j_1}^{i-1, j}, \mathbf{U}_{0, j_1}^{i, j}) =: \hat{\mathbf{F}}_{j_1}^{i-1/2, j}, & i_1 = 0, \\ \mathbf{0}, & 0 < i_1 < k, \\ \hat{\mathbf{F}}(\mathbf{U}_{k, j_1}^{i, j}, \mathbf{U}_{0, j_1}^{i+1, j}) =: \hat{\mathbf{F}}_{j_1}^{i+1/2, j}, & i_1 = k, \end{cases}$$

$$\mathbf{G}_{i_1, j_1}^{*, i, j} = \begin{cases} \hat{\mathbf{G}}(\mathbf{U}_{i_1, k}^{i, j-1}, \mathbf{U}_{i_1, 0}^{i, j}) =: \hat{\mathbf{G}}_{i_1}^{i, j-1/2}, & j_1 = 0, \\ \mathbf{0}, & 0 < j_1 < k, \\ \hat{\mathbf{G}}(\mathbf{U}_{i_1, k}^{i, j}, \mathbf{U}_{i_1, 0}^{i, j+1}) =: \hat{\mathbf{G}}_{i_1}^{i, j+1/2}, & j_1 = k. \end{cases}$$

Similar to the 1D case, the proposed 2D nodal DG scheme in each cell is designed as

$$\begin{aligned} \frac{d\mathbf{U}_{i_1,j_1}^{i,j}}{dt} = & -\frac{2}{\Delta x} \sum_{l=0}^k 2D_{i_1,l} \mathbf{F}^S(\mathbf{U}_{i_1,j_1}^{i,j}, \mathbf{U}_{l,j_1}^{i,j}) + \frac{2}{\Delta x} \frac{\tau_{i_1}}{\omega_{i_1}} (\mathbf{F}_{i_1,j_1}^{i,j} - \mathbf{F}_{i_1,j_1}^{*,i,j}) \\ & -\frac{2}{\Delta y} \sum_{l=0}^k 2D_{j_1,l} \mathbf{G}^S(\mathbf{U}_{i_1,j_1}^{i,j}, \mathbf{U}_{i_1,l}^{i,j}) + \frac{2}{\Delta y} \frac{\tau_{j_1}}{\omega_{j_1}} (\mathbf{G}_{i_1,j_1}^{i,j} - \mathbf{G}_{i_1,j_1}^{*,i,j}) + \mathbf{S}_{i_1,j_1}^{i,j}, \end{aligned} \quad (4.40)$$

where, \mathbf{F}^S and \mathbf{G}^S are the entropy conservative fluxes, $\hat{\mathbf{F}}$ and $\hat{\mathbf{G}}$ are the entropy stable fluxes,

$$\mathbf{S}_{i_1,j_1}^{i,j} = \left(0, \frac{2}{\Delta x} \rho_{i_1,j_1}^{i,j} \Theta_{i_1,j_1}^{i,j}, \frac{2}{\Delta y} \rho_{i_1,j_1}^{i,j} \Xi_{i_1,j_1}^{i,j}, \frac{2}{\Delta x} m_{i_1,j_1}^{i,j} \Theta_{i_1,j_1}^{i,j} + \frac{2}{\Delta y} n_{i_1,j_1}^{i,j} \Xi_{i_1,j_1}^{i,j} \right)^T,$$

and

$$\begin{aligned} \Theta_{i_1,j_1}^{i,j} &= \frac{1}{\rho_{i_1,j_1}^{e,i,j}} \sum_{l=0}^k 2D_{i_1,l} F_2^S(\mathbf{U}_{i_1,j_1}^{e,i,j}, \mathbf{U}_{l,j_1}^{e,i,j}), \\ \Xi_{i_1,j_1}^{i,j} &= \frac{1}{\rho_{i_1,j_1}^{e,i,j}} \sum_{l=0}^k 2D_{j_1,l} G_3^S(\mathbf{U}_{i_1,l}^{e,i,j}, \mathbf{U}_{i_1,j_1}^{e,i,j}). \end{aligned}$$

Same to the 1D case, coupling with the Euler forward time discretization, the fully-discrete scheme is given by

$$\mathbf{U}_h^{n+1} = \Pi_h^{2D}(\mathbf{U}_h^n + \Delta t \cdot \mathcal{L}_h(\mathbf{U}_h^n)) =: \Pi_h^{2D}(\mathbf{U}_h^{EF}), \quad (4.41)$$

where Π_h^{2D} is the two-dimensional scaling PP limiter to correct the density and pressure at each Gauss-Lobatto point to be positive. The definition of Π_h^{2D} is similar to Π_h in 1D (3.28). The only difference is that the stencil points on K_{ij} are $\{(X_i(x_{i_1}), Y_j(y_{j_1}))\}_{i_1,j_1=0}^k$, which is the tensor product of 1D stencil points along x - and y - directions. Note that this stencil is different from that used in [40, 41], which uses the tensor product of Gauss-Lobatto points and Gauss points. Here, we directly use the tensor product of Gauss-Lobatto points, which is a more natural and efficient choice within the nodal DG framework.

4.2 Properties of the scheme

In this section, we introduce the properties of the 2D scheme.

4.2.1 Well-balanced property

Theorem 4.1 (Well-balancedness). *The scheme (4.40) is well-balanced for a general known hydrostatic state solution $\mathbf{U}^e = (\rho^e, 0, 0, \mathcal{E}^e)$, i.e.*

$$\mathcal{L}_h(\mathbf{U}_h) = \mathbf{0}, \quad \text{if } \mathbf{U}_h = \mathbf{U}_h^e. \quad (4.42)$$

The proof follows the same procedure as the 1D case and is therefore omitted for brevity.

4.2.2 Entropy-stable property

Theorem 4.2 (Entropy-stability). *Assume the boundaries are periodic or compactly supported, then (4.40) is entropy conservative within a single element*

$$\begin{aligned} & \frac{d}{dt} \left(\frac{\Delta x \Delta y}{4} \sum_{i_1, j_1=0}^k \omega_{i_1} \omega_{j_1} \mathcal{U}(\mathbf{U}_{i_1, j_1}^{i, j}) \right) \\ &= -\frac{\Delta y}{2} \sum_{j_1=0}^k \omega_{j_1} (\mathcal{F}_{k, j_1}^{*, i, j} - \mathcal{F}_{0, j_1}^{*, i, j}) - \frac{\Delta x}{2} \sum_{i_1=0}^k \omega_{i_1} (\mathcal{G}_{i_1, k}^{*, i, j} - \mathcal{G}_{i_1, 0}^{*, i, j}), \end{aligned} \quad (4.43)$$

and ES in the sense of

$$\frac{d}{dt} \left(\frac{\Delta x \Delta y}{4} \sum_{i, j=1}^{N_x, N_y} \sum_{i_1, j_1=0}^k \omega_{i_1} \omega_{j_1} \mathcal{U}(\mathbf{U}_{i_1, j_1}^{i, j}) \right) \leq 0, \quad (4.44)$$

where

$$\begin{aligned} \mathcal{F}_{k, j_1}^{*, i, j} &= (\mathbf{V}_{k, j_1}^{i, j})^T \mathbf{F}_{k, j_1}^{*, i, j} - \psi_{F, k, j_1}^{i, j}, & \mathcal{F}_{0, j_1}^{*, i, j} &= (\mathbf{V}_{0, j_1}^{i, j})^T \mathbf{F}_{0, j_1}^{*, i, j} - \psi_{F, 0, j_1}^{i, j}, \\ \mathcal{G}_{i_1, k}^{*, i, j} &= (\mathbf{V}_{i_1, k}^{i, j})^T \mathbf{G}_{i_1, k}^{*, i, j} - \psi_{G, i_1, k}^{i, j}, & \mathcal{G}_{i_1, 0}^{*, i, j} &= (\mathbf{V}_{i_1, 0}^{i, j})^T \mathbf{G}_{i_1, 0}^{*, i, j} - \psi_{G, i_1, 0}^{i, j}. \end{aligned}$$

We omit the proof here as it is similar to the 1D case.

4.2.3 Positivity-preserving property

Theorem 4.3 (Positivity-preserving). *Given $\mathbf{U}_{i_1, j_1}^{i, j, n} \in \mathcal{G}$ on all Gauss-Lobatto quadrature points, the fully-discrete 2D scheme (4.41) satisfies $\bar{\mathbf{U}}^{i, j, n+1} \in \mathcal{G}$ under the time step*

restriction

$$\begin{aligned} \frac{\Delta t}{\Delta x} &< \min \left\{ \frac{\omega_0}{8\alpha_{x,0}}, \min \left\{ \frac{1}{4|\Theta_{i_1,j_1}^{i,j}|} \sqrt{\frac{1}{2(\gamma-1)\beta_{i_1,j_1}^{i,j}}} \right\} \right\}, & \alpha_{x,0} &= \max_{\Omega} \{|u| + c\}, \\ \frac{\Delta t}{\Delta y} &< \min \left\{ \frac{\omega_0}{8\alpha_{y,0}}, \min \left\{ \frac{1}{4|\Xi_{i_1,j_1}^{i,j}|} \sqrt{\frac{1}{2(\gamma-1)\beta_{i_1,j_1}^{i,j}}} \right\} \right\}, & \alpha_{y,0} &= \max_{\Omega} \{|v| + c\}. \end{aligned} \quad (4.45)$$

Proof. From (4.41), we derive the equation of cell averages:

$$\begin{aligned} \bar{\mathbf{U}}^{i,j,n+1} &= \bar{\mathbf{U}}^{i,j,n} - \lambda_x \sum_{j_1=0}^k \frac{\omega_{j_1}}{2} \left(\hat{\mathbf{F}}_{j_1}^{i+1/2,j} - \hat{\mathbf{F}}_{j_1}^{i-1/2,j} \right) \\ &\quad - \lambda_y \sum_{i_1=0}^k \frac{\omega_{i_1}}{2} \left(\hat{\mathbf{G}}_{i_1}^{i,j+1/2} - \hat{\mathbf{G}}_{i_1}^{i,j-1/2} \right) + \Delta t \sum_{i_1,j_1=0}^k \frac{\omega_{i_1}\omega_{j_1}}{4} \mathbf{S}_{i_1,j_1}^{i,j}, \end{aligned}$$

where $\lambda_x = \Delta t/\Delta x$, $\lambda_y = \Delta t/\Delta y$. Since $\sum_{i_1,j_1=0}^k \omega_{i_1}\omega_{j_1} = 4$, the above equation can be rewritten in the form of a convex combination

$$\begin{aligned} \bar{\mathbf{U}}^{i,j,n+1} &= \sum_{i_1=1}^{k-1} \sum_{j_1=0}^k \frac{\omega_{i_1}\omega_{j_1}}{16} \mathbf{U}_{i_1,j_1}^{i,j,n} + \sum_{i_1=0}^k \sum_{j_1=1}^{k-1} \frac{\omega_{i_1}\omega_{j_1}}{16} \mathbf{U}_{i_1,j_1}^{i,j,n} \\ &\quad + \sum_{j_1=0}^k \frac{\omega_{i_1}\omega_{j_1}}{16} \left(\mathbf{H}_{j_1}^{x,k} + \mathbf{H}_{j_1}^{x,0} \right) + \sum_{j_1=0}^k \frac{\omega_{i_1}\omega_{j_1}}{16} \left(\mathbf{H}_{i_1}^{y,k} + \mathbf{H}_{i_1}^{y,0} \right) \\ &\quad + \sum_{i_1,j_1=0}^k \frac{\omega_{i_1}\omega_{j_1}}{8} \left(\mathbf{U}_{i_1,j_1}^{i,j,n} + 2\Delta t \cdot \mathbf{S}_{i_1,j_1}^{i,j} \right), \end{aligned}$$

where

$$\begin{aligned} \mathbf{H}_{j_1}^{x,k} &= \mathbf{U}_{k,j_1}^{i,j,n} - \frac{8\lambda_x}{\omega_0} \left[\hat{\mathbf{F}} \left(\mathbf{U}_{k,j_1}^{i,j,n}, \mathbf{U}_{0,j_1}^{i+1,j,n} \right) - \hat{\mathbf{F}} \left(\mathbf{U}_{0,j_1}^{i,j,n}, \mathbf{U}_{k,j_1}^{i,j,n} \right) \right], \\ \mathbf{H}_{j_1}^{x,0} &= \mathbf{U}_{0,j_1}^{i,j,n} - \frac{8\lambda_x}{\omega_0} \left[\hat{\mathbf{F}} \left(\mathbf{U}_{0,j_1}^{i,j,n}, \mathbf{U}_{k,j_1}^{i,j,n} \right) - \hat{\mathbf{F}} \left(\mathbf{U}_{k,j_1}^{i-1,j,n}, \mathbf{U}_{0,j_1}^{i,j,n} \right) \right], \\ \mathbf{H}_{i_1}^{y,k} &= \mathbf{U}_{i_1,k}^{i,j,n} - \frac{8\lambda_y}{\omega_0} \left[\hat{\mathbf{G}} \left(\mathbf{U}_{i_1,k}^{i,j,n}, \mathbf{U}_{i_1,0}^{i,j+1,n} \right) - \hat{\mathbf{G}} \left(\mathbf{U}_{i_1,0}^{i,j,n}, \mathbf{U}_{i_1,k}^{i,j,n} \right) \right], \\ \mathbf{H}_{i_1}^{y,0} &= \mathbf{U}_{i_1,0}^{i,j,n} - \frac{8\lambda_y}{\omega_0} \left[\hat{\mathbf{G}} \left(\mathbf{U}_{i_1,0}^{i,j,n}, \mathbf{U}_{i_1,k}^{i,j,n} \right) - \hat{\mathbf{G}} \left(\mathbf{U}_{i_1,k}^{i,j-1,n}, \mathbf{U}_{i_1,0}^{i,j,n} \right) \right]. \end{aligned}$$

Hence, if we have $\mathbf{H} \in \mathcal{G}$ for all \mathbf{H} , and $\mathbf{U}_{i_1,j_1}^{i,j,n} + 2\Delta t \cdot \mathbf{S}_{i_1,j_1}^{i,j} \in \mathcal{G}$ for all i_1, j_1 , then we can obtain $\bar{\mathbf{U}}^{i,j,n+1} \in \mathcal{G}$ by the convexity of \mathcal{G} . For the \mathbf{H} terms, we have that they all

belong to \mathcal{G} if

$$\frac{8\lambda_x}{\omega_0}\alpha_{x,0} \leq 1, \quad \frac{8\lambda_y}{\omega_0}\alpha_{y,0} \leq 1.$$

For the source term, we omit the subscripts i, j, i_1, j_1, n for brevity and define

$$\mathbf{U}^* := \mathbf{U} + 2\Delta t \cdot \mathbf{S} = \begin{bmatrix} \rho \\ m + 4\lambda_x\rho\Theta \\ n + 4\lambda_y\rho\Xi \\ \mathcal{E} + 4\lambda_x m\Theta + 4\lambda_y n\Xi \end{bmatrix}.$$

Similar to the 1D case, the density of state \mathbf{U}^* is positive, and hence $\mathbf{U}^* \in \mathcal{G}$ if and only if its pressure is also positive, i.e.,

$$\mathcal{E} + 4\lambda_x m\Theta + 4\lambda_y n\Xi - \frac{(m + 4\lambda_x\rho\Theta)^2 + (n + 4\lambda_y\rho\Xi)^2}{2\rho} > 0.$$

The solution of above inequality is

$$\lambda_x^2\Theta^2 + \lambda_y^2\Xi^2 < \frac{1}{16(\gamma - 1)\beta}. \quad (4.46)$$

It is easy to verify that (4.46) holds under the CFL condition (4.45). \square

Remark 4.1. *We want to remark that the 2D PP limiter does not increase the total entropy as well.*

5 Numerical experiments

In this section, we present numerical results for the proposed method to demonstrate its high-order accuracy for smooth solutions, as well as its WB, ES, and PP properties. Unless otherwise noted, we only show results with $k = 2$. The ten-stage, fourth-order SSP-RK method developed by Ketcheson [24] is used for time discretization, with time step

$$\Delta t = \frac{\text{CFL}}{\alpha_{x,0}}\Delta x, \quad \text{or} \quad \Delta t = \frac{\text{CFL}}{\alpha_{x,0}/\Delta x + \alpha_{y,0}/\Delta y}, \quad \text{CFL} = 0.5,$$

and hence the CFL condition for the PP property (3.36) or (4.45) is satisfied. Note that, to demonstrate the reliability and robustness of the proposed scheme, no slope limiters are employed in any of the tests. Our method, denoted as ‘‘WBESPP,’’ is compared against the following three methods to highlight its advantages in preserving simultaneously the WB, ES, and PP properties. Specifically, for the 1D case, these schemes are defined as follows:

(a) “non-WB” method with the semi-discrete formulation

$$\frac{\Delta x}{2} \frac{d\mathbf{U}_{i_1}^i}{dt} + \sum_{l=0}^k 2D_{i_1,l} \mathbf{F}^S(\mathbf{U}_{i_1}^i, \mathbf{U}_l^i) + \frac{\tau_{i_1}}{\omega_{i_1}} (\mathbf{F}_{i_1}^{*,i} - \mathbf{F}_{i_1}^i) = \frac{\Delta x}{2} \mathbf{S}(\mathbf{U}_{i_1}^i, x_i(X_{i_1})).$$

Note that the scheme is ES due to $(\mathbf{V}_{i_1}^i)^T \mathbf{S}(\mathbf{U}_{i_1}^i, x_i(X_{i_1})) = 0$. The limiter Π_h is applied. Hence, the non-WB scheme is ES and PP but not WB.

(b) “non-ES” method with the semi-discrete formulation

$$\frac{\Delta x}{2} \frac{d\mathbf{U}_{i_1}^i}{dt} + \sum_{l=0}^k D_{i_1,l} \mathbf{F}_l^i + \frac{\tau_{i_1}}{\omega_{i_1}} (\mathbf{F}_{i_1}^{*,i} - \mathbf{F}_{i_1}^i) = \tilde{\mathbf{S}}_{i_1}^i,$$

where

$$\tilde{\mathbf{S}}_{i_1}^i = \left(0, \rho_{i_1}^i \tilde{\Theta}_{i_1}^i, m_{i_1}^i \tilde{\Theta}_{i_1}^i \right), \quad \tilde{\Theta}_{i_1}^i = \frac{1}{\rho_{i_1}^{e,i}} \sum_{l=0}^k D_{i_1,l} F_{2,l}^{i_1}.$$

The PP limiter Π_h is employed. The non-ES scheme is WB and PP but not ES.

(c) “non-PP” method with the same formulation as (3.22). While the PP limiter Π_h is not used. Hence, the non-PP scheme is WB and ES but not PP.

5.1 One-dimensional tests

Example 5.1 (Well-balancedness test.) In this example, we consider different steady states and test the well-balanced property of the proposed scheme. We take $\gamma = 5/3$ and $\Omega = [0, 2]$ in this example. Under the linear gravitational potential $\phi_x = 1$, we consider both the isothermal and the isentropic steady state solutions, which are respectively given by

$$\text{Eqbm1: } \rho^e(x) = \exp(-x), \quad p^e(x) = \exp(-x),$$

$$\text{Eqbm2: } \rho^e(x) = \left(\rho_0^{\gamma-1} - \frac{1}{K_0} \frac{\gamma-1}{\gamma} gx \right)^{\frac{1}{\gamma-1}}, \quad p^e(x) = K_0 (\rho^e(x))^\gamma.$$

The parameters for Eqbm2 are set as $\rho_0 = 1$, $g = 1$, $K_0 = 1$. One can easily check that both of them satisfy (2.5) and will lead to the exact balance of the flux and the source term.

First, we take the steady state solution as initial condition and compute the solution until time $T = 4$. In Tab. 5.1, we present the errors of density of different schemes. It is notable that these errors are calculated between the numerical solutions \mathbf{U}_h^n and the interpolating polynomials of steady state solutions \mathbf{U}_h^e . We can see that errors of our

WBESPP scheme are all at the level of round-off error both for the isothermal equilibrium and the polytropic equilibrium, demonstrating the desired WB property independent of the specific type of the equilibrium. While the non-WB scheme shows the expected third order accuracy of the scheme.

Next, we add a small perturbation to Eqbm2 at the left boundary $x = 0$ to show the advantage of WB scheme in simulating the evolution of such small perturbation. The perturbation is added on the velocity, which is given by $u(0, t) = 10^{-6} \sin(4\pi t)$. The solutions are computed until time $T = 1.5$, at which point the waves have not yet propagated to the right boundary. In Fig. 5.1, we present the pressure perturbation and velocity on $N = 200$ meshes against the reference solution computed by the WBPP method [14] on $N = 2000$ meshes. One can see that the results with the WB scheme agree well with the reference solution, while the results by the non-WB scheme has a large error especially for $x > 1.5$. Thus indicates that the WB method is more accurate for resolving small perturbation to steady states.

Table 5.1. Example 5.1: One-dimensional well-balancedness test. Errors and orders of density at final time $T = 4$ for $k = 2$.

	N	L^1 error	order	L^2 error	order	L^∞ error	order
WBESPP							
Eqbm1	20	1.67e-15	–	2.09e-15	–	5.55e-15	–
	40	3.10e-15	–	3.95e-15	–	1.11e-14	–
	80	5.42e-15	–	7.04e-15	–	2.08e-14	–
	160	1.41e-14	–	1.66e-14	–	5.96e-14	–
Eqbm2	20	1.56e-15	–	2.57e-15	–	9.21e-15	–
	40	4.43e-15	–	6.34e-15	–	2.13e-14	–
	80	8.08e-15	–	1.10e-14	–	3.54e-14	–
	160	1.56e-14	–	2.20e-14	–	6.94e-14	–
non-WB							
Eqbm1	20	7.01e-06	–	9.02e-06	–	3.30e-05	–
	40	9.03e-07	2.96	1.17e-06	2.95	4.44e-06	2.89
	80	1.15e-07	2.98	1.49e-07	2.97	5.77e-07	2.95
	160	1.44e-08	2.99	1.88e-08	2.99	7.35e-08	2.97
Eqbm2	20	3.34e-06	–	3.75e-06	–	9.44e-06	–
	40	4.36e-07	2.94	4.95e-07	2.92	1.29e-06	2.87
	80	5.58e-08	2.97	6.36e-08	2.96	1.69e-07	2.93
	160	7.05e-09	2.98	8.07e-09	2.98	2.17e-08	2.96

Example 5.2 (Sod shock tube.) Here, we test the 1D Sod-like shock tube problem with the gravitational potential $\phi_x = 1$, which is a standard test example for Euler equation, and is originally introduced in [32]. The computational domain is taken as

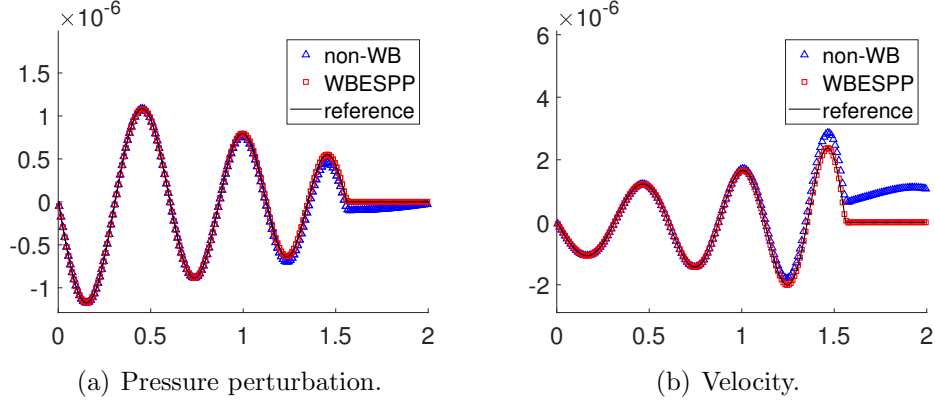


Figure 5.1. Example 5.1: One-dimensional well-balancedness test with small velocity perturbation. The numerical solution at $T = 1.5$ on $N = 200$ meshes.

$\Omega = [-1, 1]$ with reflective boundaries on both sides, and the initial data is given by

$$(\rho, u, p) = \begin{cases} (1, 0, 1), & x < 0, \\ (0.125, 0, 0.1), & x \geq 0. \end{cases}$$

In Fig. 5.2, we present the result of density at $T = 0.4$ on $N = 200$ meshes. The reference solution is computed by the WBPP method [14] with TVB limiter on $N = 1200$ meshes. Due to the entropy stability, we can see the discontinuities are captured sharply and stably, although we do not add the shock limiter. While the computation will break down before the final time without ES treatment. In Fig. 5.3, we present the time evolution of total entropy for our WBESPP scheme and non-ES scheme. It can be observed that the ES treatment indeed dissipates the total entropy.

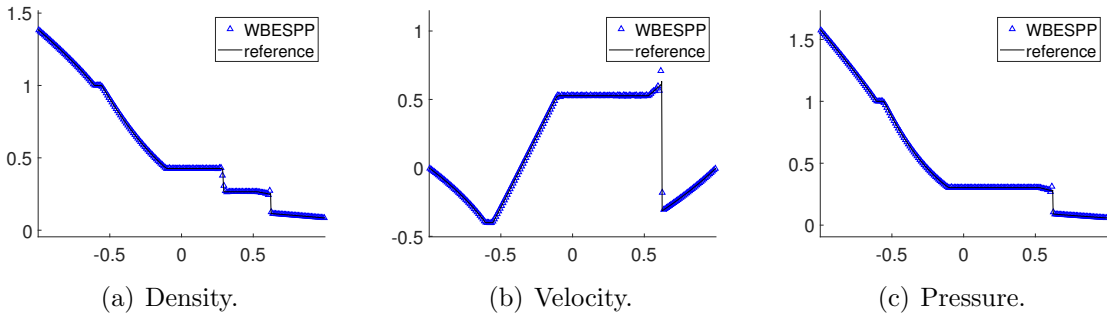


Figure 5.2. Example 5.2: One-dimensional Sod-like shock tube. The numerical solution at $T = 0.4$ on $N = 200$ meshes.

Example 5.3 (Double rarefaction.) We consider the double rarefaction problem with the gravitational potential $\phi_x = x$. This example includes extreme low density and

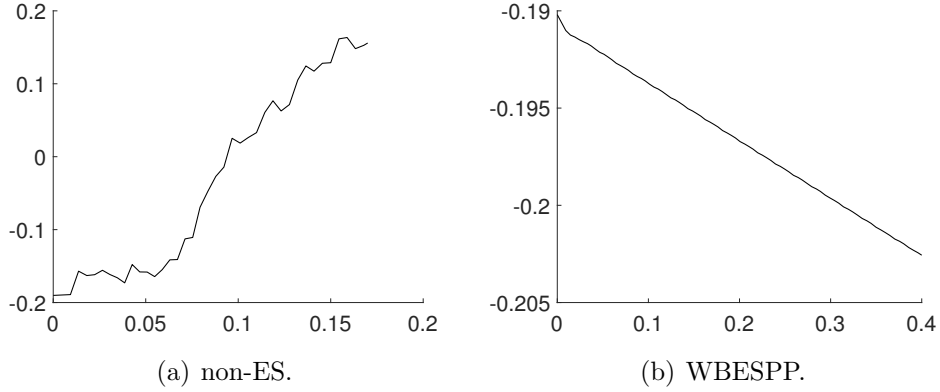


Figure 5.3. Example 5.2: One-dimensional Sod-like shock tube. The evolution of total entropy on $N = 200$ meshes.

pressure. The computational domain is taken as $\Omega = [-1, 1]$ with outflow boundaries, and the initial data is given as

$$(\rho, u, p) = \begin{cases} (7, -1, 0.2), & x < 0, \\ (7, 1, 0.2), & x \geq 0. \end{cases}$$

We run the simulation until $T = 0.6$ on $N = 800$ meshes, and the results are shown in Fig. 5.4. The reference solution is computed by the WBPP method [14] on $N = 1600$ meshes. We can see that the structure of solution is resolved well, while the density and pressure are preserved to be positive. We want to remark that the computation will break down at the first step without the PP treatment since the negative density and pressure are introduced.

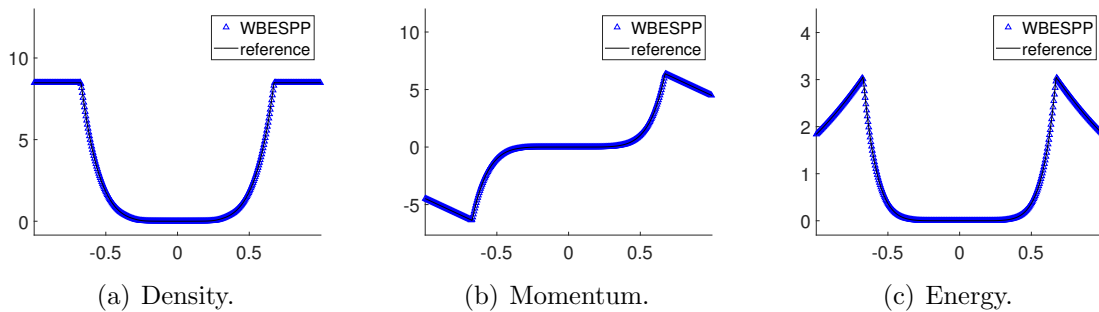


Figure 5.4. Example 5.3: One-dimensional double rarefaction problem. The numerical solution at $T = 0.6$ on $N = 800$ meshes.

5.2 Two-dimensional tests

Example 5.4 (Well-balancedness test.) We consider the two-dimensional isothermal steady state solution in [36] under the linear gravitational potential $\phi_x = \phi_y = g$. The exact steady state solution is given by

$$\rho^e = \rho_0 \exp\left(-\frac{\rho_0 g}{p_0}(x+y)\right), \quad \mathbf{u}^e = \mathbf{0}, \quad p^e = p_0 \exp\left(-\frac{\rho_0 g}{p_0}(x+y)\right),$$

where the parameters are $\rho_0 = 1.21$, $p_0 = 1$, $g = 1$. The computational domain is taken as $\Omega = [0, 1] \times [0, 1]$.

We first take the initial data as the steady state solution and compute the solution until $T = 1$. In Tab. 5.2, we present the errors of density, demonstrating that our proposed WBESPP scheme also maintains the balance errors at machine level for the 2D problem.

Next, we add a small perturbation on pressure

$$p = p^e + 0.001 \exp\left(-100((x-0.3)^2 + (y-0.3)^2)\right).$$

In Fig. 5.5, we present the results of density perturbation and pressure perturbation at $T = 0.15$ on mesh with $N_x \times N_y = 100 \times 100$. It is observed that the non-WB scheme can not capture those small perturbations well, while the WB method resolves them accurately.

Table 5.2. Example 5.4: Two-dimensional well-balancedness test. Errors and orders of density at final time $T = 1$.

	$N_x = N_y$	L^1 error	order	L^2 error	order	L^∞ error	order
WBESPP	20	7.08e-15	–	8.05e-15	–	2.80e-14	–
	40	1.40e-14	–	1.56e-14	–	5.88e-14	–
	80	2.81e-14	–	3.13e-14	–	1.12e-13	–
	160	5.72e-14	–	6.38e-14	–	2.19e-13	–
non-WB	20	1.31e-06	–	1.53e-06	–	9.10e-06	–
	40	1.65e-07	2.98	1.93e-07	2.98	1.21e-06	2.91
	80	2.08e-08	2.99	2.43e-08	2.99	1.58e-07	2.94
	160	2.60e-09	3.00	3.05e-09	3.00	2.01e-08	2.97

Example 5.5 (Accuracy test.) In this example, we test the accuracy of the scheme with the gravitational potential $\phi_x = \phi_y = 1$. The computational domain is taken as $\Omega = [0, 2\pi] \times [0, 2\pi]$, and the exact smooth solution is given by

$$\rho = 1 + 0.2 \sin(x + y - 2t), \quad u = v = 1, \quad p = 20 - x - y + 2t + 0.2 \cos(x + y - 2t).$$

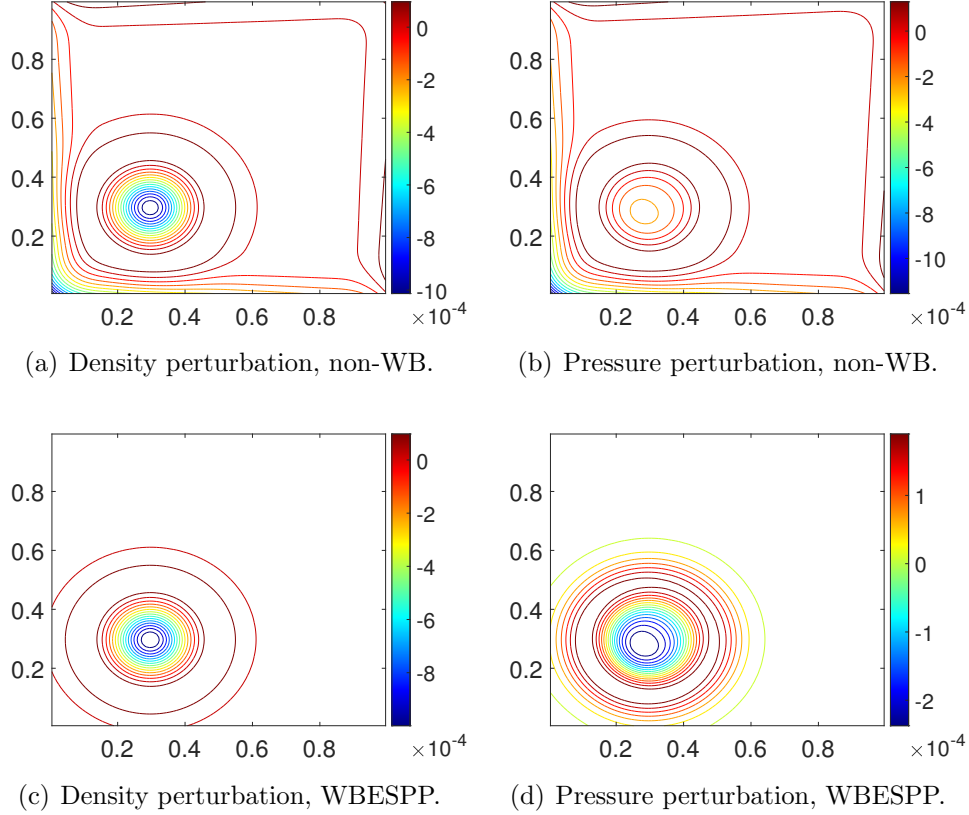


Figure 5.5. Example 5.4: Two-dimensional well-balancedness test. The numerical solution at $T = 0.15$ on $N_x \times N_y = 100 \times 100$ meshes. 15 contour lines are used.

We run the simulation up to $T = 0.5$. In Tab. 5.3, we present the errors and orders of density for $k = 1, 2, 3$, and the optimal $(k + 1)$ -th convergence rates are observed.

Example 5.6 (Double rarefaction.) Here, we consider the two-dimensional double rarefaction test in [23], which is used to demonstrate the positivity-preserving property of a scheme. The computational domain is $\Omega = [-0.5, 0.5] \times [-0.5, 0.5]$ with the gravitational potential $\phi = 0.5(x^2 + y^2)$. The initial data is given by

$$\rho = \exp(-\phi(x, y)/0.4), \quad p = 0.4 \exp(-\phi(x, y)/0.4),$$

$$u = \begin{cases} -2, & x \leq 0, \\ 2, & x > 0, \end{cases} \quad v = 0.$$

We run the simulation until $T = 0.1$ on $N_x \times N_y = 200 \times 200$ meshes, and the results are shown in Fig. 5.6. It can be seen that the WBESPP scheme can compute this problem stably. We note that for the non-PP scheme, the computation will break down at first several steps.

Table 5.3. Example 5.5: Two-dimensional accuracy test. Errors and orders of density at final time $T = 0.5$.

	$N_x = N_y$	L^1 error	order	L^2 error	order	L^∞ error	order
$k = 1$	20	2.73e-03	–	3.16e-03	–	6.69e-03	–
	40	7.00e-04	1.96	8.06e-04	1.97	1.94e-03	1.79
	80	1.76e-04	1.99	2.02e-04	2.00	5.20e-04	1.90
	160	4.40e-05	2.00	5.03e-05	2.00	1.34e-04	1.96
$k = 2$	20	2.77e-04	–	3.53e-04	–	1.25e-03	–
	40	5.21e-05	2.41	6.65e-05	2.41	2.33e-04	2.43
	80	8.30e-06	2.65	1.06e-05	2.65	3.63e-05	2.68
	160	1.16e-06	2.84	1.48e-06	2.84	4.95e-06	2.87
$k = 3$	20	1.51e-06	–	2.07e-06	–	1.74e-05	–
	40	7.61e-08	4.31	1.05e-07	4.30	9.16e-07	4.25
	80	5.09e-09	3.90	7.10e-09	3.89	6.25e-08	3.87
	160	2.47e-10	4.36	4.36e-10	4.02	3.12e-09	4.32

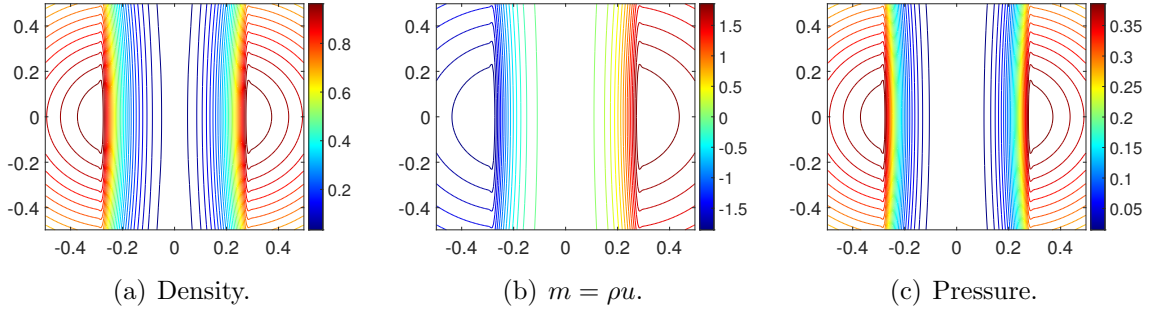


Figure 5.6. Example 5.6: Two-dimensional double rarefaction test. The numerical solution at $T = 0.1$ on $N_x \times N_y = 200 \times 200$ meshes. 30 contour lines are used.

Example 5.7 (Radial Rayleigh-Taylor instability.) In this example, we simulate the radial Rayleigh-Taylor instability problem with the gravitational potential $\phi = r = \sqrt{x^2 + y^2}$. The initial data is

$$\rho = \begin{cases} \exp(-r), & r < r_0, \\ \exp\left(-\frac{r}{\alpha} + r_0 \frac{1-\alpha}{\alpha}\right), & r > r_0, \end{cases} \quad p = \begin{cases} \exp(-r), & r < r_i, \\ \frac{1}{\alpha} \exp\left(-\frac{r}{\alpha} + r_0 \frac{1-\alpha}{\alpha}\right), & r > r_i, \end{cases}$$

where the parameters are given by

$$r_i = \eta(1 + \cos(k\theta)), \quad \alpha = \exp(r_0)/(\exp(r_0) + \Delta_\rho), \quad \theta = \arctan(y/x),$$

and $r_0 = 6$, $\eta = 0.02$, $\Delta_\rho = 0.1$, $k = 20$. The equilibrium state is set to $\rho^e = p^e =$

$\exp(-r)$. We can see that in the regions $r < r_0(1 - \eta)$ and $r > r_0(1 + \eta)$, the initial condition is in stable equilibrium. But due to the discontinuous density, a Rayleigh-Taylor instability will develop near the interface $r = r_i(\theta)$ at $t \approx 2.5$. Meanwhile, the solution is closed to the equilibrium state at the location away from the interface.

In Fig. 5.7, we plot the result of density perturbation at $T = 2.9, 3.8, 5$ on $N_x \times N_y = 240 \times 240$ meshes. One can see that both two schemes produce relatively accurate results with the instabilities concentrated near the location of the interface. Thanks to the ES property, the computation is stable without applying the shock limiter. Moreover, it is notable that the computation will break down at $t = 2.41$ without the ES treatment.

However, it seems that there are some non-physical structures appearing in the central area by non-WB scheme. The enlarged results at $T = 5$ near the center are shown in Fig. 5.8. It can be seen that the perturbation of the non-WB scheme is about 10^{-3} level without the ring structure, while the level is 10^{-4} for WBESPP scheme, indicates that our scheme can better retain the equilibrium solution away from the interface.

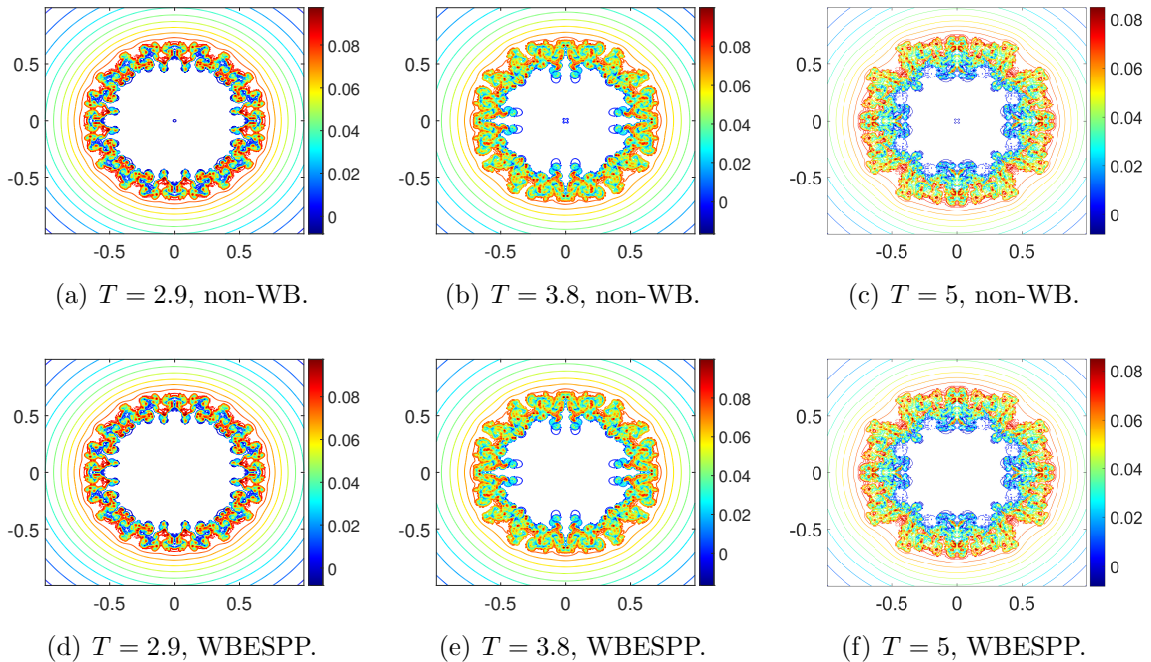


Figure 5.7. Example 5.7: Two-dimensional radial Rayleigh-Taylor instability. The density perturbation on $N_x \times N_y = 240 \times 240$ meshes. 10 contour lines are used.

Example 5.8 (Inertia-gravity wave problem.) Finally, we consider the inertia-gravity wave problem studied in [16], which is a benchmark test problem arising from atmospheric flows. This problem involves the evolution of a potential temperature perturbation in a channel which is of interest in the validation of numerical weather prediction schemes. The computational domain is a $\Omega = [0, 300000] \times [0, 10000]$ m² rectangle with periodic boundaries on the left and right edges, and reflective boundaries on the top

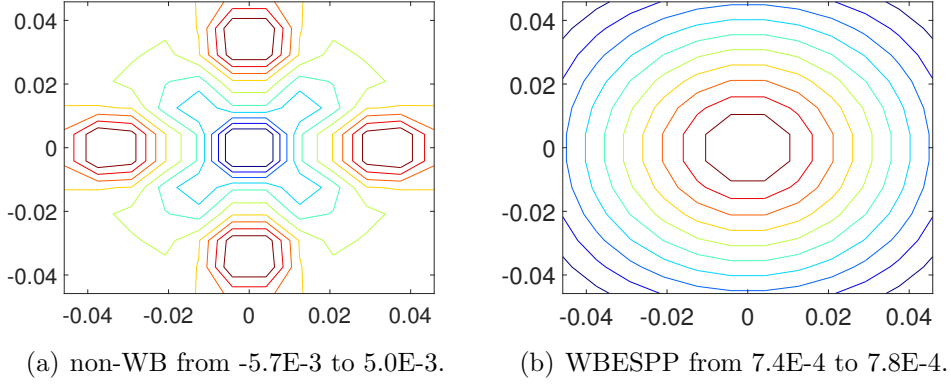


Figure 5.8. Example 5.7: Two-dimensional radial Rayleigh-Taylor instability. The density perturbation at $T = 5$ around central area on $N_x \times N_y = 240 \times 240$ meshes. 10 contour lines are used.

and bottom edges. The gravity function of this problem is $\phi = gy$, $g = 9.8 \text{ m/s}^2$. The equilibrium solution is given by

$$\rho^e = \frac{p_0}{R\Theta^e} \Pi^{\frac{1}{\gamma-1}}, \quad \mathbf{u}^e = \mathbf{0}, \quad p^e = p_0 \Pi^{\frac{\gamma}{\gamma-1}},$$

where

$$\Theta^e = T_0 \exp\left(\frac{\mathcal{N}^2 y}{g}\right), \quad \Pi = 1 + \frac{(\gamma-1)g^2}{\gamma R T_0 \mathcal{N}} \left[\exp\left(-\frac{\mathcal{N}^2 y}{g}\right) - 1 \right].$$

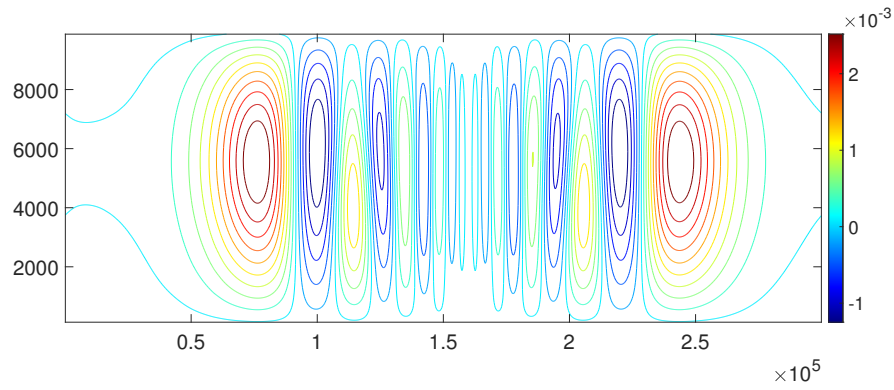
The parameters are $p_0 = 10^5 \text{ N/m}^2$, $T_0 = 300 \text{ K}$, $\mathcal{N} = 0.01/\text{s}$, $R = 287.058 \text{ J/kg K}$. Then, a small perturbation is added to the potential temperature Θ :

$$\Delta\Theta_0 = \theta_c \sin\left(\frac{\pi y}{h_c}\right) \left[1 + \left(\frac{x-x_c}{a_c}\right)^2 \right]^{-1},$$

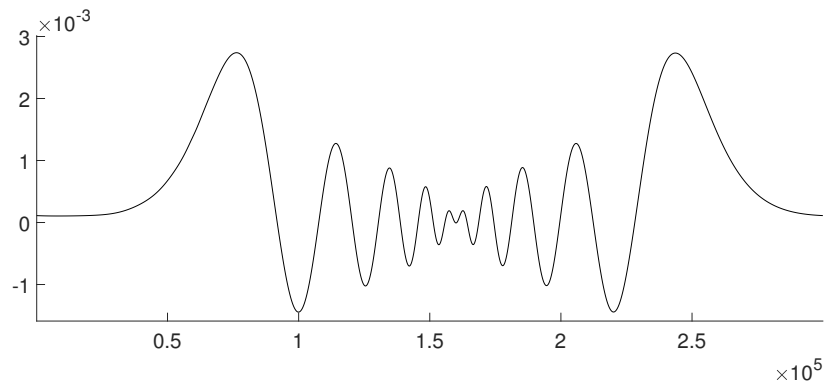
where $\theta_c = 0.01 \text{ K}$, $h_c = 10000 \text{ m}$, $x_c = 100000 \text{ m}$, $a_c = 5000 \text{ m}$. The initial data for ρ and p are given by

$$\rho = \frac{p_0}{R(\Theta^e + \Delta\Theta_0)} \Pi^{\frac{1}{\gamma-1}}, \quad p = p^e,$$

and the velocity is set to $u = 20 \text{ m/s}$, $v = 0$. In Fig. 5.9, we present the result of the potential temperature perturbation $\Delta\Theta$ at $T = 3000 \text{ s}$ on $N_x \times N_y = 1200 \times 40$ meshes. Compare to the results in [16], one can see that the evolution of potential temperature perturbation is resolved well by the proposed WBESPP scheme.



(a) Overview.



(b) Cut at $y = 5000$.

Figure 5.9. Example 5.8: Inertia-gravity wave problem. The potential temperature perturbation at $T = 3000$ s on $N_x \times N_y = 1200 \times 40$ meshes. 10 contour lines are used.

6 Concluding remarks

In this paper, we propose a structure preserving nodal DG scheme for solving the Euler equations with gravity which is well-balanced, entropy stable, and positivity-preserving. By rewriting the balance law and modifying the discretization of source term using an entropy conservative flux, we are able to achieve both the well-balancedness and entropy stability simultaneously. With a positivity preserving scaling limiter, we demonstrate that the fully-discrete scheme coupled with the forward Euler scheme ensures the positivity of density and pressure. Moreover, the limiter does not destroy the entropy stability and well-balancedness. Theoretical analysis and numerical results confirm that our scheme maintains the numerical equilibrium state to machine accuracy, dissipates entropy, and preserves positive density and pressure even in extreme cases. Future works include the extension to unstructured meshes, and the application of other equations.

References

- [1] R. Abgrall. A general framework to construct schemes satisfying additional conservation relations. Application to entropy conservative and entropy dissipative schemes. *Journal of Computational Physics*, 372:640–666, 2018.
- [2] K. Arun and M. Kar. An energy stable well-balanced scheme for the barotropic Euler system with gravity under the anelastic scaling. *Numerical Methods for Partial Differential Equations*, 41(1):e23168, 2025.
- [3] A. Bollermann, G. Chen, A. Kurganov, and S. Noelle. A well-balanced reconstruction of wet/dry fronts for the shallow water equations. *Journal of Scientific Computing*, 56:267–290, 2013.
- [4] P. Chandrashekar. Kinetic energy preserving and entropy stable finite volume schemes for compressible Euler and Navier-Stokes equations. *Communications in Computational Physics*, 14(5):1252–1286, 2013.
- [5] P. Chandrashekar and C. Klingenberg. A second order well-balanced finite volume scheme for Euler equations with gravity. *SIAM Journal on Scientific Computing*, 37(3):B382–B402, 2015.
- [6] P. Chandrashekar and M. Zenk. Well-balanced nodal discontinuous Galerkin method for Euler equations with gravity. *Journal of Scientific Computing*, 71(3):1062–1093, 2017.
- [7] T. Chen and C.-W. Shu. Entropy stable high order discontinuous Galerkin methods with suitable quadrature rules for hyperbolic conservation laws. *Journal of Computational Physics*, 345:427–461, 2017.

- [8] B. Cockburn, S. Hou, and C.-W. Shu. The Runge-Kutta local projection discontinuous Galerkin finite element method for conservation laws. IV. The multidimensional case. *Mathematics of Computation*, 54(190):545–581, 1990.
- [9] B. Cockburn, S.-Y. Lin, and C.-W. Shu. TVB Runge-Kutta local projection discontinuous Galerkin finite element method for conservation laws III: one-dimensional systems. *Journal of computational Physics*, 84(1):90–113, 1989.
- [10] B. Cockburn and C.-W. Shu. TVB Runge-Kutta local projection discontinuous Galerkin finite element method for conservation laws. II. General framework. *Mathematics of computation*, 52(186):411–435, 1989.
- [11] B. Cockburn and C.-W. Shu. The Runge-Kutta local projection-discontinuous-Galerkin finite element method for scalar conservation laws. *ESAIM: Mathematical Modelling and Numerical Analysis*, 25(3):337–361, 1991.
- [12] A. Del Grosso, M. J. Castro, A. Chan, G. Gallice, R. Loubère, and P.-H. Maire. A well-balanced, positive, entropy-stable, and multi-dimensional-aware finite volume scheme for 2D shallow-water equations with unstructured grids. *Journal of Computational Physics*, 503:112829, 2024.
- [13] V. Desveaux, M. Zenk, C. Berthon, and C. Klingenberg. A well-balanced scheme to capture non-explicit steady states in the Euler equations with gravity. *International Journal for Numerical Methods in Fluids*, 81(2):104–127, 2016.
- [14] J. Du, Y. Yang, and F. Zhu. Well-balanced positivity-preserving high-order discontinuous Galerkin methods for Euler equations with gravitation. *Journal of Computational Physics*, 505:112877, 2024.
- [15] E. Gaburro, P. Öffner, M. Ricchiuto, and D. Torlo. High order entropy preserving ADER-DG schemes. *Applied Mathematics and Computation*, 440:127644, 2023.
- [16] F. X. Giraldo and M. Restelli. A study of spectral element and discontinuous Galerkin methods for the Navier–Stokes equations in nonhydrostatic mesoscale atmospheric modeling: Equation sets and test cases. *Journal of Computational Physics*, 227(8):3849–3877, 2008.
- [17] E. Godlewski and P.-A. Raviart. *Numerical approximation of hyperbolic systems of conservation laws*, volume 118. Springer Science & Business Media, 2013.
- [18] S. K. Godunov. An interesting class of quasilinear systems. In *Dokl. Akad. Nauk SSSR*, volume 139, pages 521–523, 1961.
- [19] L. Grosheintz-Laval and R. Käppeli. High-order well-balanced finite volume schemes for the Euler equations with gravitation. *Journal of Computational Physics*, 378:324–343, 2019.

- [20] J.-L. Guermond and B. Popov. Fast estimation from above of the maximum wave speed in the Riemann problem for the Euler equations. *Journal of Computational Physics*, 321:908–926, 2016.
- [21] A. Harten. On the symmetric form of systems of conservation laws with entropy. *Journal of Computational Physics*, 49(1):151–164, 1983.
- [22] T. Hughes, L. Franca, and M. Mallet. A new finite element formulation for computational fluid dynamics: I. Symmetric forms of the compressible Euler and Navier-Stokes equations and the second law of thermodynamics. *Computer Methods in Applied Mechanics and Engineering*, 54(2):223–234, 1986.
- [23] H. Jiang, H. Tang, and K. Wu. Positivity-preserving well-balanced central discontinuous Galerkin schemes for the Euler equations under gravitational fields. *Journal of Computational Physics*, 463:111297, 2022.
- [24] D. I. Ketcheson. Highly efficient strong stability-preserving Runge–Kutta methods with low-storage implementations. *SIAM Journal on Scientific Computing*, 30(4):2113–2136, 2008.
- [25] G. Li and Y. Xing. Well-balanced discontinuous Galerkin methods for the Euler equations under gravitational fields. *Journal of Scientific Computing*, 67:493–513, 2016.
- [26] Y. Liu, W. Guo, Y. Jiang, and M. Zhang. Non-oscillatory entropy stable DG schemes for hyperbolic conservation law. *arXiv preprint arXiv:2410.16729*, 2024.
- [27] Y. Liu, W. Guo, Y. Jiang, and M. Zhang. A globally divergence-free entropy stable nodal DG method for conservative ideal MHD equations. *arXiv preprint arXiv:2501.06815*, 2025.
- [28] Y. Liu, C.-W. Shu, and M. Zhang. Entropy stable high order discontinuous Galerkin methods for ideal compressible MHD on structured meshes. *Journal of Computational Physics*, 354:163–178, 2018.
- [29] V. Michel-Dansac, C. Berthon, S. Clain, and F. Foucher. A well-balanced scheme for the shallow-water equations with topography. *Computers & Mathematics with Applications*, 72(3):568–593, 2016.
- [30] W. H. Reed and T. R. Hill. Triangular mesh methods for the neutron transport equation. Technical report, Los Alamos Scientific Lab., N. Mex.(USA), 1973.
- [31] J. P. Slotnick, A. Khodadoust, J. Alonso, D. Darmofal, W. Gropp, E. Lurie, and D. J. Mavriplis. CFD vision 2030 study: a path to revolutionary computational aerosciences. Technical report, 2014.

- [32] G. A. Sod. A survey of several finite difference methods for systems of nonlinear hyperbolic conservation laws. *Journal of Computational Physics*, 27(1):1–31, 1978.
- [33] E. F. Toro. *Riemann solvers and numerical methods for fluid dynamics: a practical introduction*. Springer Science & Business Media, 2013.
- [34] M. Waruszewski, J. E. Kozdon, L. C. Wilcox, T. H. Gibson, and F. X. Giraldo. Entropy stable discontinuous Galerkin methods for balance laws in non-conservative form: Applications to the Euler equations with gravity. *Journal of Computational Physics*, 468:111507, 2022.
- [35] K. Wu and Y. Xing. Uniformly high-order structure-preserving discontinuous Galerkin methods for Euler equations with gravitation: Positivity and well-balancedness. *SIAM Journal on Scientific Computing*, 43(1):A472–A510, 2021.
- [36] Y. Xing and C.-W. Shu. High order well-balanced WENO scheme for the gas dynamics equations under gravitational fields. *Journal of Scientific Computing*, 54:645–662, 2013.
- [37] Y. Xing, C.-W. Shu, and S. Noelle. On the advantage of well-balanced schemes for moving-water equilibria of the shallow water equations. *Journal of scientific computing*, 48(1):339–349, 2011.
- [38] Y. Xing, X. Zhang, and C.-W. Shu. Positivity-preserving high order well-balanced discontinuous Galerkin methods for the shallow water equations. *Advances in Water Resources*, 33(12):1476–1493, 2010.
- [39] Z. Xu and C.-W. Shu. A high-order well-balanced discontinuous Galerkin method for hyperbolic balance laws based on the Gauss-Lobatto quadrature rules. *Journal of Scientific Computing*, 101(2):39, 2024.
- [40] X. Zhang and C.-W. Shu. On positivity-preserving high order discontinuous Galerkin schemes for compressible Euler equations on rectangular meshes. *Journal of Computational Physics*, 229(23):8918–8934, 2010.
- [41] X. Zhang and C.-W. Shu. Positivity-preserving high order discontinuous Galerkin schemes for compressible Euler equations with source terms. *Journal of Computational Physics*, 230(4):1238–1248, 2011.